Behavior of the Space Charge In a Plasma Magnetron

by
Y. Ikeda

Series No. 60, Issue No. 433
Contract No. AF 19(628)-324
June 15, 1962

ELECTRONICS RESEARCH LABORATORY

"Requesters for additional copies by Agencies of the Department of Defense, their contractors, and other Government agencies should be directed to the:

ARMED SERVICES TECHNICAL INFORMATION AGENCY
ARLINGTON HALL STATION
ARLINGTON 12, VIRGINIA

Department of Defense contractors must be established for ASTIA services or have their 'need-to-know' certified by the cognizant military agency of their project or contract."

"All other persons and organizations should apply to the:

U.S. DEPARTMENT OF COMMERCE
OFFICE OF TECHNICAL SERVICES
WASHINGTON 25, D.C."

AFCRL-63-41

Electronics Research Laboratory
University of California
Berkeley, California

BEHAVIOR OF THE SPACE CHARGE IN A PLASMA MAGNETRON

by

Y. Ikeda

Institute of Engineering Research
Series No. 60, Issue No. 433

Contract No. AF 19(628)-324
Project No. 5634
Task No. 563402

Scientific Report No. 17

June 15, 1962

Prepared for
Electronics Research Directorate
Air Force Cambridge Research Laboratories
Office of Aerospace Research
United States Air Force
Bedford, Massachusetts

ACKNOWLEDGMENT

The author is indebted to the Electronics Research Laboratory of the University of California, Berkeley, for providing him with the opportunity of doing the research. The investigation was carried out under the guidance of Prof. D. H. Sloan. The author appreciates the useful discussions with Prof. Sloan and also gratefully acknowledges the suggestions made by Profs. A. J. Lichtenberg and C. Süsskind with regard to the final manuscript, as well as the technical assistance provided by O. B. Westwick and M. Chamran.

ABSTRACT

An analytical and experimental investigation of "plasma" magnetrons with smooth-bore anodes is described. Secondary-emission yield of several materials is investigated and the region in which limiting anode currents are obtained is related to the operation of conventional magnetrons. Basic phenomena caused by Philips-ion-gage discharge particles are described, with particular emphasis on the sheath region. The phenomena underlying the build-up of anode current are elucidated.

TABLE OF CONTENTS

LIST OF FIGURES

LIST OF FIGURES

LIST OF TABLES

I. INTRODUCTION

The magnetron with a distributed-emission cathode has been shown to convert dc to ac with high efficiency.[1,2] Plasma-magnetrons with smooth-bore anodes have been investigated for the purpose of increasing the output power of magnetrons as well as for exploring the plasma boundary in a magnetic field.[3]

The behavior of such tubes depends largely on the secondary-emission yield of the cathode material. The higher-yield cathode is used with lower anode voltages, where appreciable turbulent flow into the anode occurs even under very good vacuum conditions. With lower-yield secondary-emission cathodes, the anode-voltage can be increased to a fairly high value without any appreciable anode current. In the latter case, many of the carriers are supplied through an ionization process.

The region where the anode current increases rapidly with the anode voltage for an aluminum or a magnesium cathode, which has a high secondary-emission ratio, should be related to the operation of usual magnetrons. This region has been investigated for the purpose of getting optimum dimensions of the interaction space.[3,4] A region where the anode-voltage builds up without an appreciable anode current, as obtained with a stainless-steel cathode which has a comparatively low secondary-emission yield, may be interesting for another reason. The high-energy particles, which move back and forth along the curved magnetic-field lines owing to PIG action, may cause a high kinetic temperature in the plasma.[3,5]

The experiments to be described were planned to investigate the basic phenomena caused by the PIG-discharge particles, with particular emphasis on investigating the sheath region. Though magnetron structures were used for the experiment, it may be possible to replace one metal boundary with a plasma. In this situation both electron and ion sheaths are possible, depending on the potentials. Although only metal boundaries are discussed in this report, it may also provide some basic information about

the ion sheath as the counterpart of the electron sheath.

The most interesting results have been obtained in the investigation of the space-charge behavior of a magnetron with a stainless-steel cathode. Since the low secondary-emission yield of the stainless-steel cathode allows the anode voltage to be increased to more than a few tens of kilovolts without an appreciable anode current, many interesting phenomena have been revealed that were previously hidden behind the build-up of the anode current in magnetrons with aluminum or magnesium cathodes.

As an application to the investigation of the motion of particles in crossed fields, the values of the fields for optimal bunching in a magnetron are also obtained.

All formulas are in MKS units unless otherwise specified.

II. EXPERIMENTAL PROCEDURE

The experimental equipment used is shown schematically in Fig. 1. The noise at the anode, the cage-current characteristics,

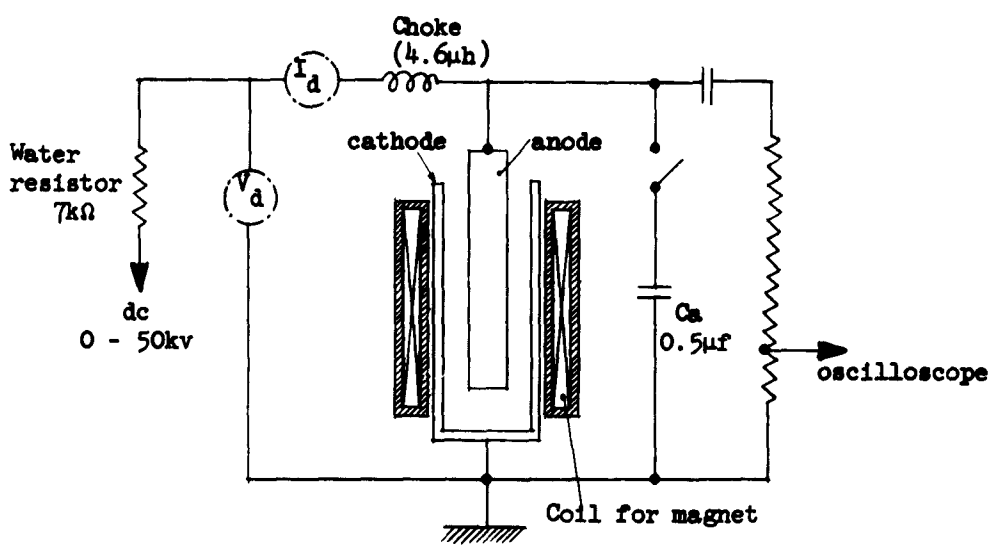

Fig. 1.--Schematic of experimental equipment.

and the frequency spectra in a given frequency region were measured as the experimental factors of primary interest. The relation between anode voltage and anode current under various magnetic fields was also investigated.

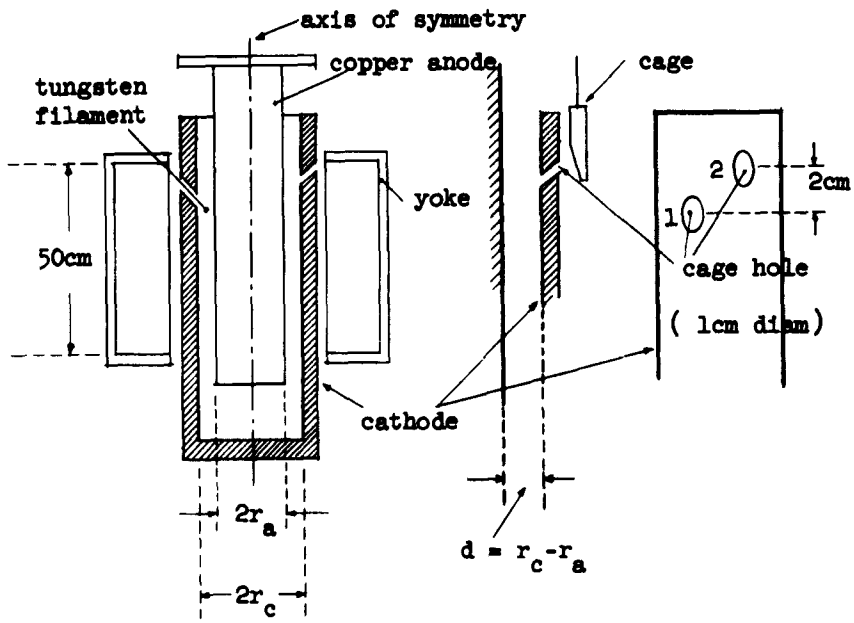

Fig. 2.--Illustration of devices tested.

The devices tested are shown in Fig. 2. The data relating to the three devices, which are described in Table 1, will be presented in the following pages. The cages installed in their

TABLE I.--Devices tested.

Symbol of device	Cathode material	$2r_c$ (cm)	$2r_a$ (cm)	d (cm)	Number of cages	Tungsten filament
SS-2.4	Stainless Steel	15.26	10.5	2.4	2	yes
SS-1.1	Stainless Steel	15.26	13.0	1.1	2	yes
Al-2.45	Aluminum	15.4	10.5	2.45	3	no

respective devices are numbered from the one nearest to the central part of the device. They are used for diagnosing the character of PIG-discharge electrons in the interaction space. A tungsten

filament, projecting several millimeters from the stainless-steel cathode into the anode-cathode space, at the cage position, is used for detecting the frequency spectra of PIG-discharge current. (It was installed originally to provide more electrons, to compensate for small secondary emission.)

The value of the magnetic field produced by the magnet coil refers to the central part of the device. If nothing is noted about the anode condenser (C_a = 0.5 μf), it may be understood that it is removed from the equipment. A hydrogen leak issued for controlling the gas pressure inside the devices (SS-2.4) and (SS-1.1).

III. RELATIONS AMONG ANODE VOLTAGE, ANODE CURRENT, AND MAGNETIC FIELD

Voltage-current characteristics for (SS-2.4) are illustrated in Fig. 3 with magnetic field and hydrogen pressure as parameters;

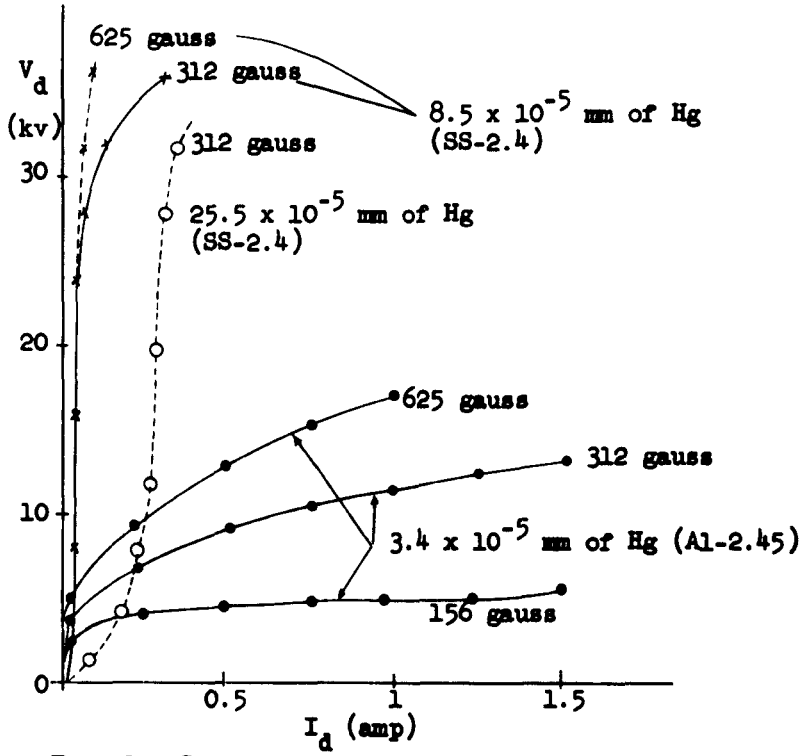

Fig. 3.--Comparison of voltage-current characteristics for (SS-2.4) and (Al-2.45).

they are compared with the characteristics for (Al-2.45). The difference between the secondary-emission yields of the stainless-steel and the aluminum cathodes accounts for the markedly different characteristics. The hydrogen pressure does not greatly affect the value of anode voltage where the anode current builds up abruptly for (SS-2.4). A relation between anode current and gas pressure is shown in Fig. 4, which gives a linear dependence of I_d on p (pressure).

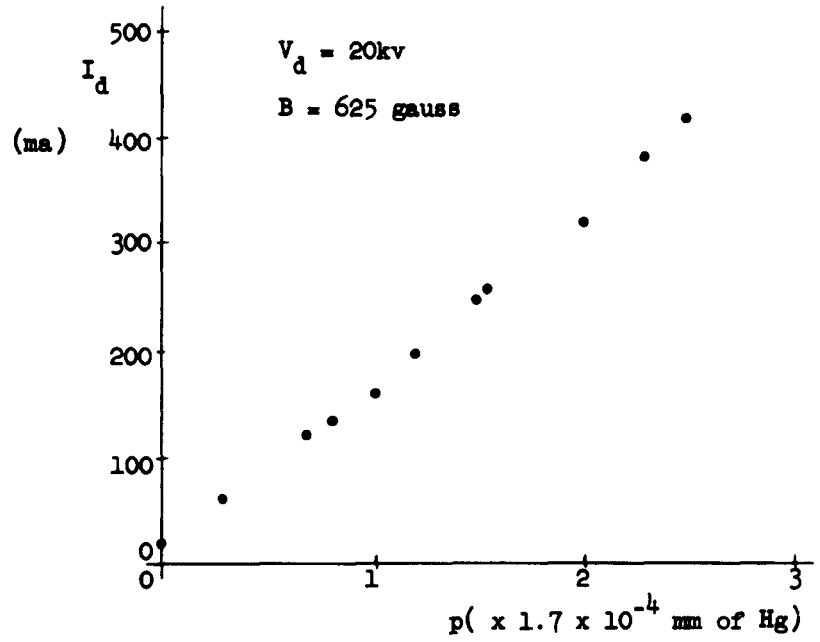

Fig. 4.--Illustration of linear dependence of I_d on p.

From Figs. 3 and 4 we see that the I-V characteristic does not appreciably change with pressure, except for the smooth increase in current at a given voltage. From this result we may infer that the basic space-charge pattern in the crossed-field region is not greatly affected by the gas pressure (measurements have been made below 10^{-3} mm of Hg) but the electron scattering

towards the anode is affected by the pressure.[7] This result is easily conceivable if the magnetic pressure is considered to be much higher than the gas pressure. Suppose V_a = 10 kV, B = 0.0312 weber/m^2, and a laminar-flow situation holds. A simple calculation shows that the electron circulating current amounts to 28.7 amp/m, which determines the difference between the magnetic fields at anode side and at cathode side in the gap region. The corresponding difference of the pressures at both sides may be expressed as

$$\Delta p \simeq B \cdot \Delta H \qquad (1)$$

where ΔH is given by the circulating current. If B = 0.0312 weber/m^2 and ΔH = 28.7 amp/m, $\Delta p \simeq 0.9$ N/$m^2 \simeq$ 70 μHg. This calculation illustrates the fact that much higher density of ions than that given by the gas pressure does exist on the surface of the cathode.

The voltage-current characteristics for the (SS-1.1) device, whose separation distance between anode and cathode is about half that of (SS-2.4), are illustrated in Figs. 5 and 6.

The bumps in the I-V characteristic for the narrow spacing were not found in the previously discussed devices. However, the symptoms of these irregularities are found even in the (SS-2.4) device when noise-measurements are made with it. These irregularities are described in the latter sections.

The crest value of the anode current at a bump increases with gas pressure and the corresponding voltage is determined only by the magnetic field. The value of both the voltage and the current at the crest increases with increasing magnetic field. The crest value may be considered to correspond to the "maximum-current boundary" for the device. It is strongly affected by the surface condition of the electrode. If the secondary-emission ratio of a surface is very high the maximum-current boundary becomes correspondingly large. With the aluminum cathode, for example, it was not attainable owing to power limitations.

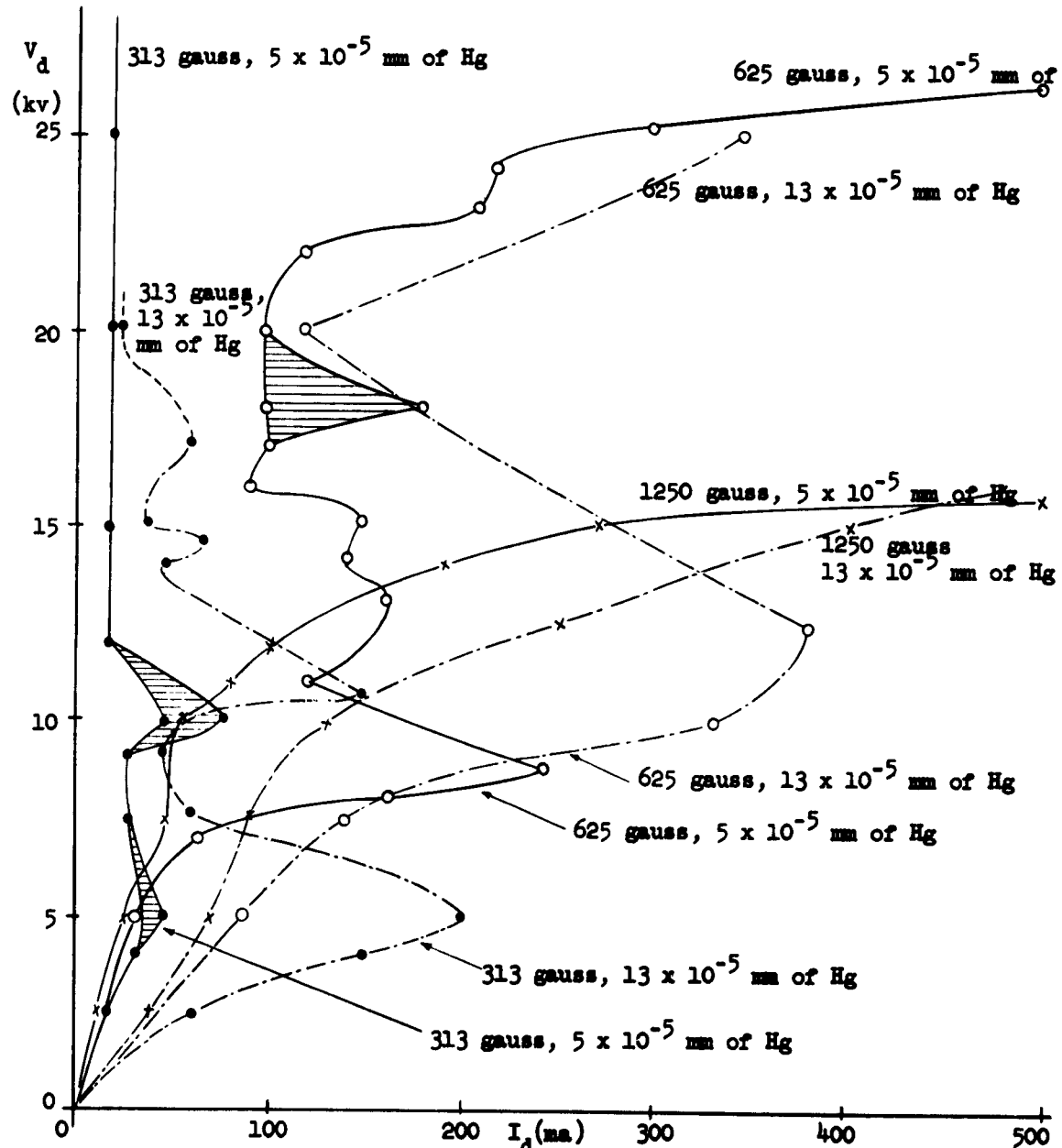

Fig. 5.--Voltage-current characteristics for (SS-1.1) without anode condenser.

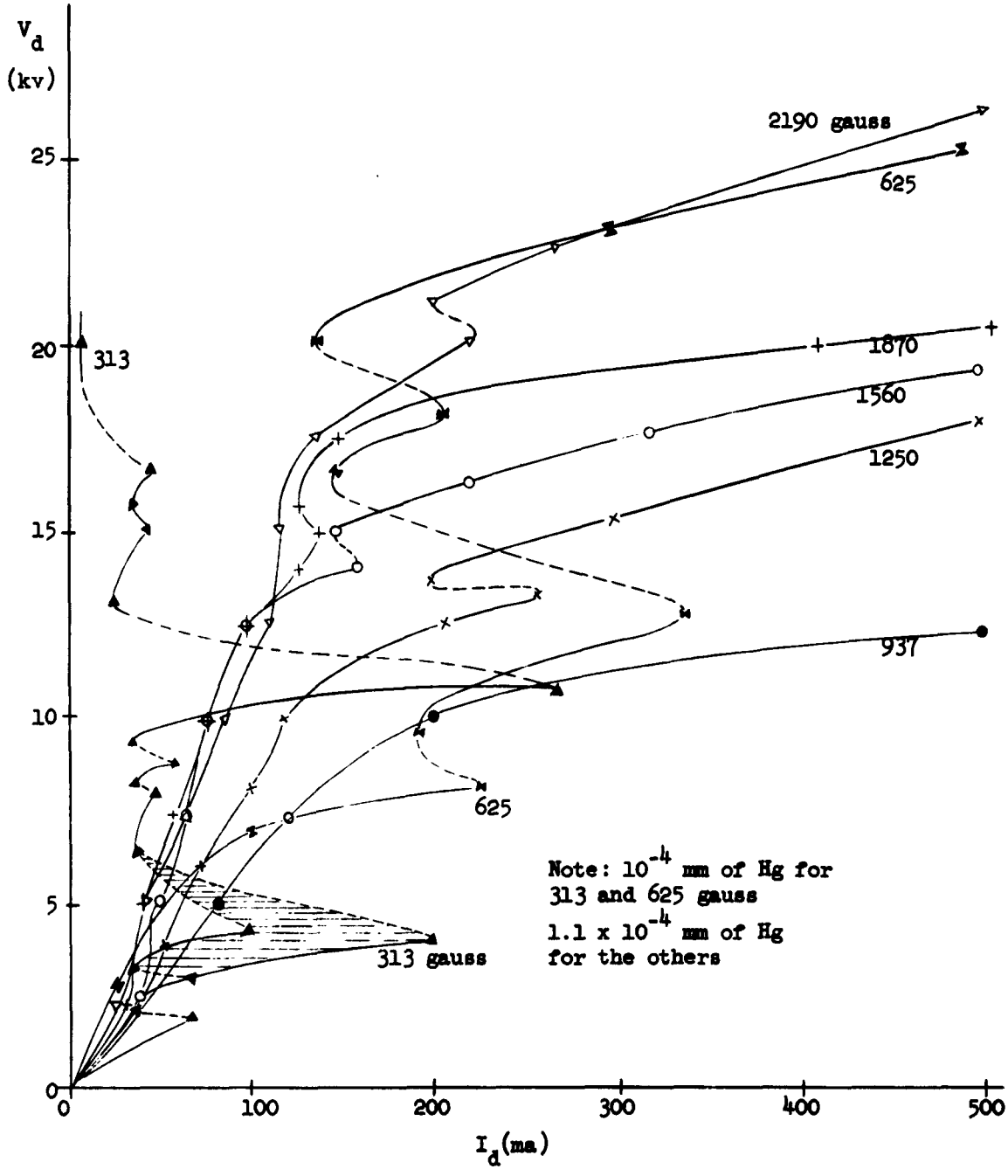

Fig. 6.--Voltage-current characteristics for (SS-1.1) with anode condenser.

IV. NOISE AT ANODE

The noise component of the anode voltage was measured with an oscilloscope and the approximate effective value is plotted as a function of the dc anode voltage and the magnetic field in Figs. 7 through 12. Since the pattern of the anode noise is quite variable, as shown in Fig. 10, a value of noise voltage read from an ordinate has only a qualitative meaning.

The data in Figs. 7 and 11 are taken without anode condenser for the (SS-2.4) and (SS-1.1) devices, respectively; the high noise voltage observed has usually a fundamental frequency in the range from several tens to a few hundreds of kilocycles. This large amplitude of noise has no particular dependence on the dc anode voltage, magnetic field and hydrogen pressure. The anode capacitance of 0.5 μf can stop the large variation of the anode voltage, as is clear from Figs. 8, 9, 10, and 12. The noise component, in this case, previously hidden behind the large amplitude of low-frequency noise, appears over the higher-frequency region. The condenser, which is effective in shorting the noise voltage in the hundred-kilocycle region, behaves like an inductive reactance for the megacycle noise frequencies. The noise observed with the condenser inserted is characterized by a fundamental frequency in the range beyond about 10 Mc and by being modulated with a frequency between several tens and a few hundreds of kilocycles.

The correlations between Figs. 11 and 5 and between Figs. 12 and 6 are remarkable in that the peaks in anode current are always accompanied by the peaks in anode noise. It should be particularly emphasized that the positions of the noise curve peaks in the lower magnetic-field region (shown in Figs. 7, 8, 11, and 12) change approximately as a function of V_d/B^2. Some typical examples are indicated with the marks of arrows connected by dotted lines. The V_d/B^2 value is kept constant along each dotted line. On the other hand it appears that the V_d/B value is kept constant in the higher magnetic-field region as shown by the simple arrowmarks in Fig. 7.

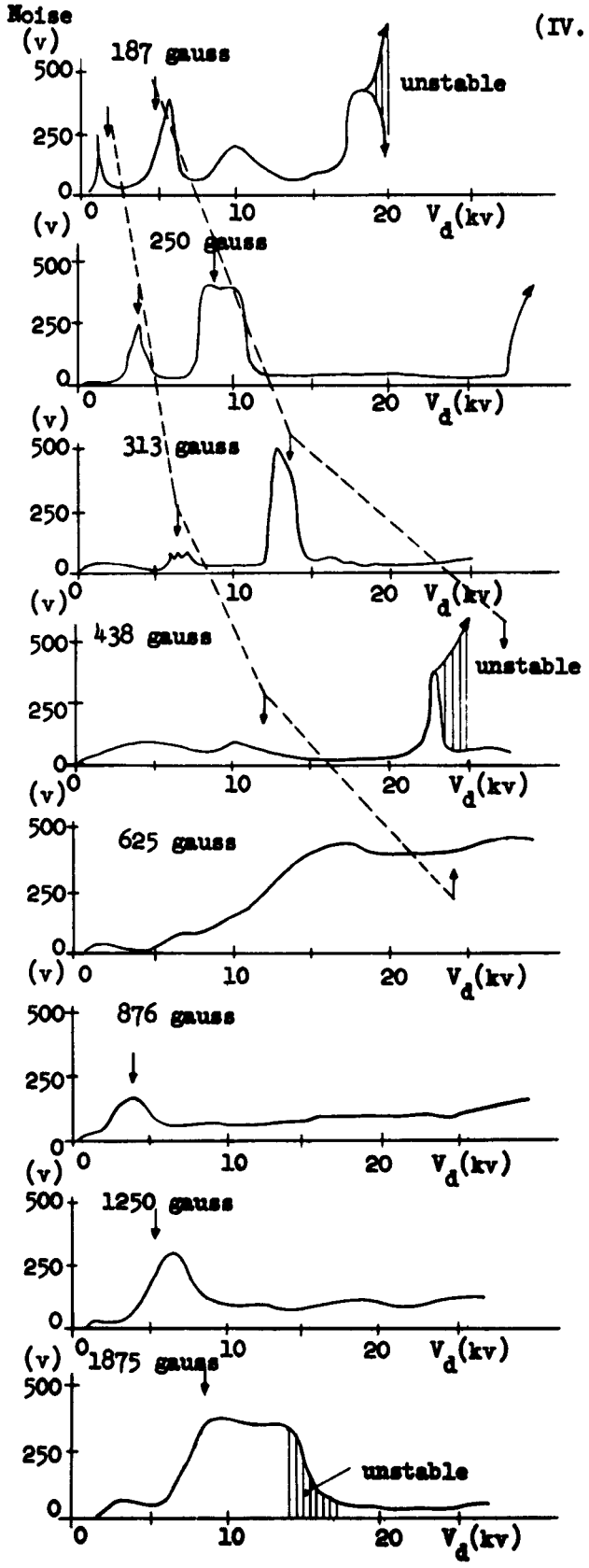

Fig. 7.--Anode noise characteristics without anode condenser at 1.7×10^{-4} mm of Hg for (88-2.4).

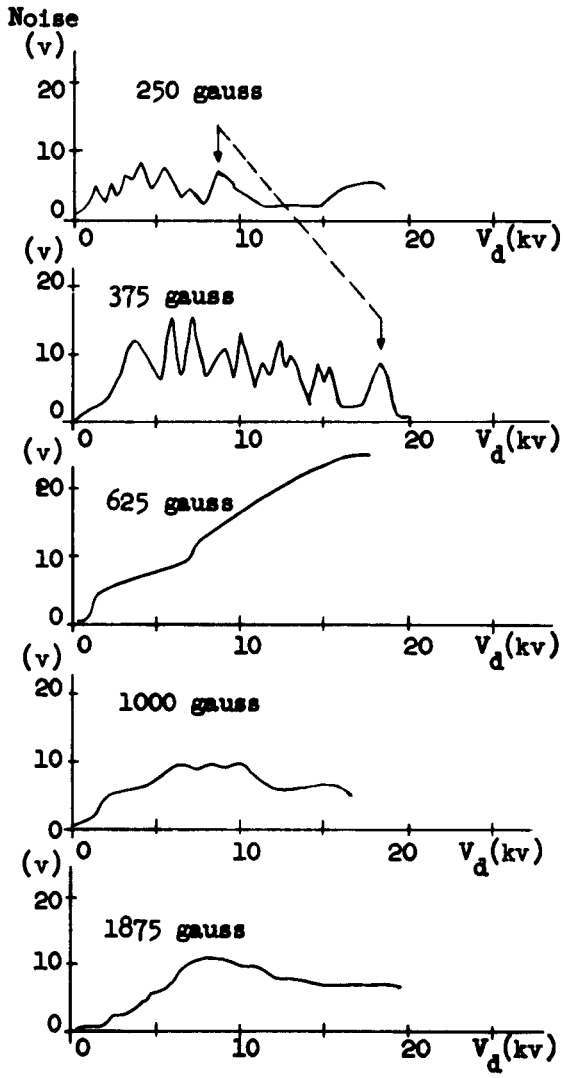

Fig. 8.--Anode noise characteristics with anode condenser at 1.7×10^{-4} mm of Hg for (SS-2.4).

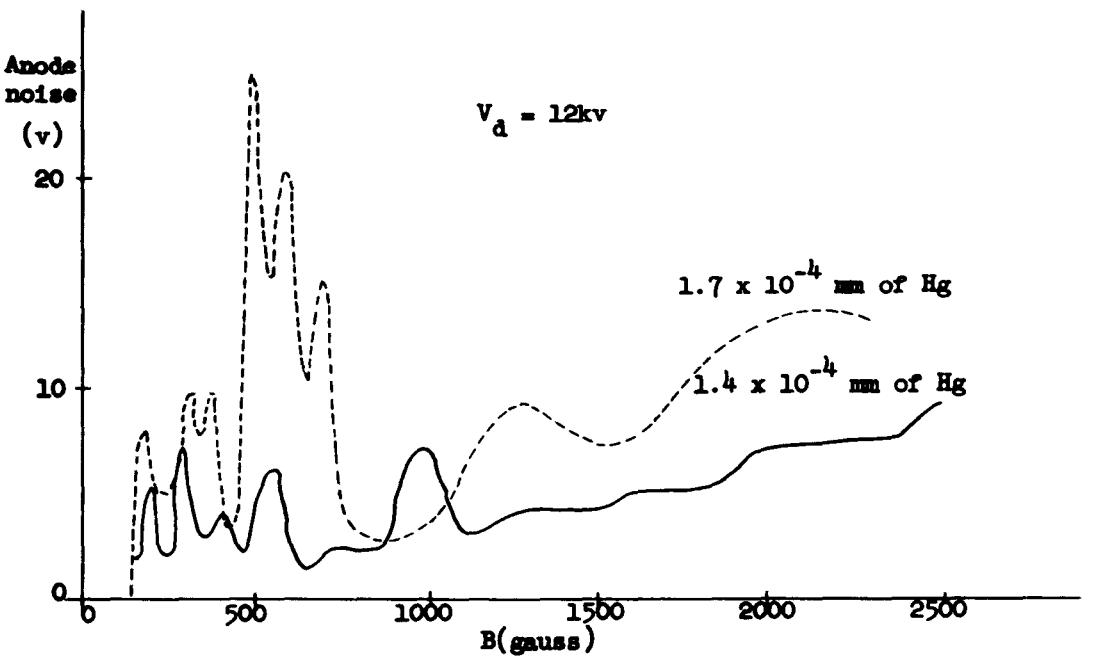

Fig. 9.--Anode noise characteristics with anode condenser for (SS-2.4).

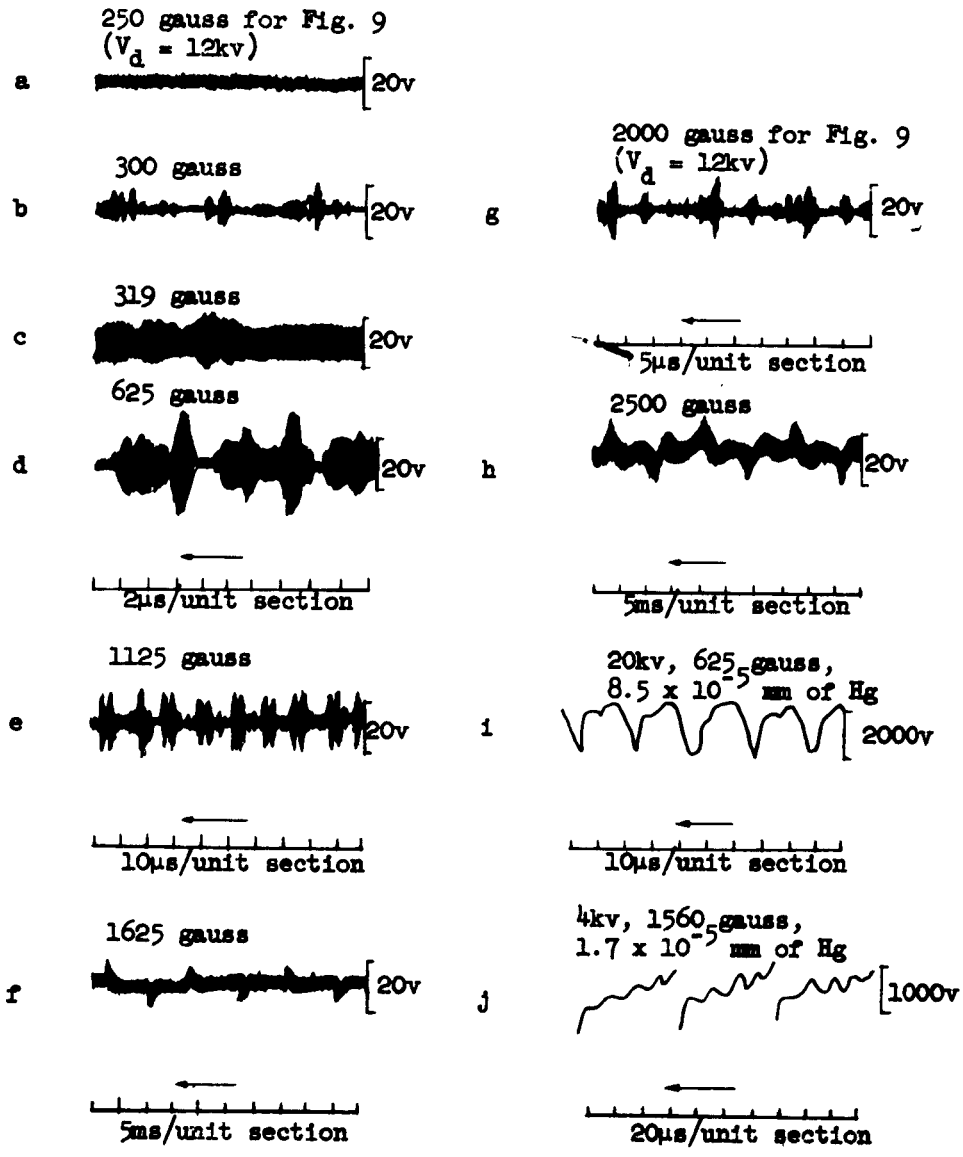

Fig. 10.--Anode noise patterns for (88-2.4):
a-h, with anode condenser (12kv,
1.4 x 10^{-4} mm of Hg);
i-j, without anode condenser.

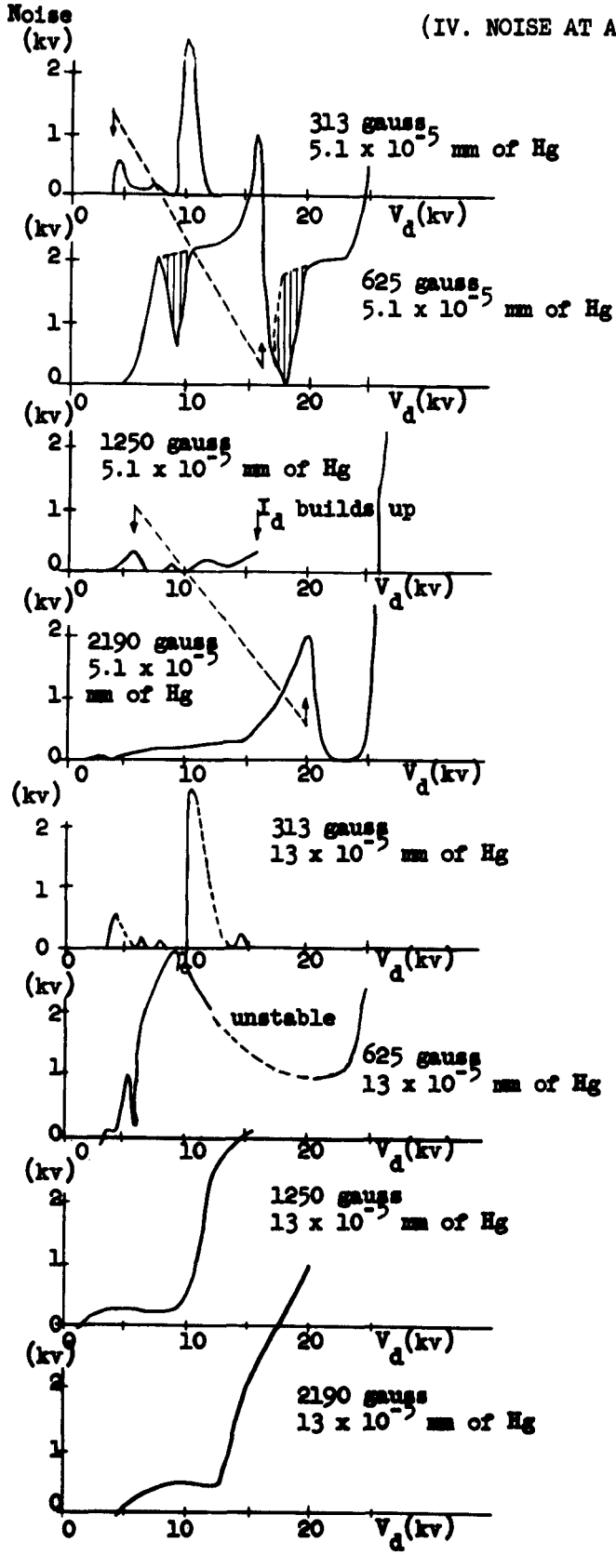

Fig. 11.--Anode noise characteristics without anode condenser for (SS-1.1).

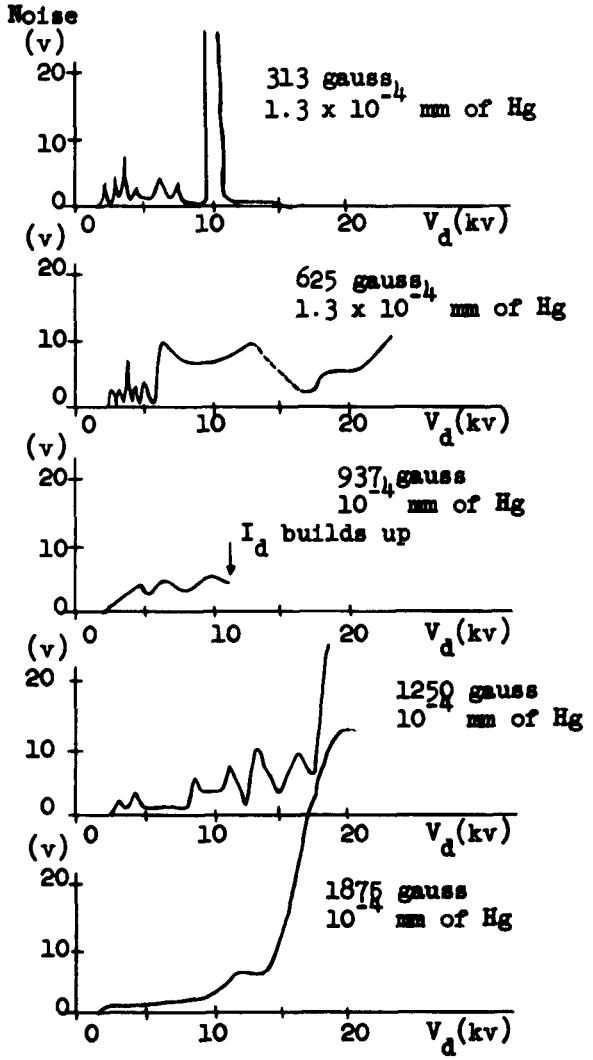

Fig. 12.--Anode noise characteristics with anode condenser for (SS-1.1).

The high-frequency components of the modulated wave patterns shown in Fig. 10 were not investigated systematically, because of measurement difficulties. However, it has been observed that the frequency ranges over a band of a few tens of megacycles, and does not change appreciably with the magnetic field or the anode voltage. Occasionally it increases a little with the anode voltage. Also occasionally it was found to change in proportion to the drift velocity.

The value of the frequency of about 100 kc, which is observed as the anode noise without the anode condenser, is not caused by the external circuit, as discussed below. The capacitance between anode and cathode(ground), which is estimated to be a few hundred picofarads, and the water-resistor of about 7 K at the anode circuit correspond to a time constant of about 1 μsec--about the same as the restoring time of the anode voltage in Fig. 10-i. The probable cause of the large amplitude of noise is a periodic ion-depletion, where the period is mainly determined by a diffusion time for the neutral gas from the cathode area to the anode area. The succeeding ionization process is expected to occur and cease comparatively rapidly. The following numerical calculation tends to support this assumption. Suppose the temperature of the neutral gas is 100°C (since the electrodes are water cooled): the average velocity in the radial direction is

$$\bar{v}_r = \sqrt{2\,k\,T/\pi\,m_g} \simeq 1400 \text{ m/sec}$$

for the hydrogen-atom gas. This value requires about 17 μsec for an atom to pass through the whole separation distance between anode and cathode of the (88-2.4) device. If we compare this time with the period of the relaxation oscillation in Fig. 10-i, for example, we see that the two times agree fairly well.

If the anode voltage is relatively small in terms of the magnetic field, the cyclotron diameter of an ion can become smaller than the separation distance between anode and cathode and it may stay in the interaction space for a relatively long time. A plasma layer may be expected around the cathode for this situation

and various kinds of plasma instabilities may occur.[8] The voltage pattern shown in Fig. 10-j may be attributed to this kind of phenomenon.

V. OBSERVATIONS OF NOISE WITH TUNGSTEN PROBE

Since the anode noise is only indirectly related to the circumferential motion of the electrons, direct measurements of this motion cannot be obtained from the external circuit. A probe should therefore be used for the further investigation of the space-charge behavior. Figure 13 shows examples of the frequency spectra of the tungsten-probe noise. Though similar behavior is observed with the anode noise as well as with the cage noise, the tungsten probe was found to be most useful for the measurement of the effects of the circulating electron beam. Circulating frequencies are indicated in the figure that are calculated from the familiar relation[9]

$$f_{cir} = \frac{f_c}{2}\left[1 - \sqrt{1 - (V_d/V_c)}\right] \qquad (2)$$

where f_c is the cyclotron frequency of electron and V_c is the cutoff voltage of the magnetron.

From Fig. 13(a) to (f), the anode voltage is fixed at 20 kv and the magnetic field is taken as the parameter. It may be noted that a sharp peak noise is found in the region near 438 gauss, and a broad peak noise exists in the region near 1500 gauss. The results of various observations including Fig. 13 signify that there are many modes over a wide frequency range in the cavity space and that some of them are excited by the circulating electron beam. If the frequency of a mode is related to the circulating frequency by an integral ratio, the mode is strongly excited. Since many modes are distributed over a broad frequency range, the noise-spectrum patterns appear to be modulated with the circulating frequency and its harmonics.

If the anode voltage and the magnetic field are in a certain relation the noise is very large, which seems to indicate the

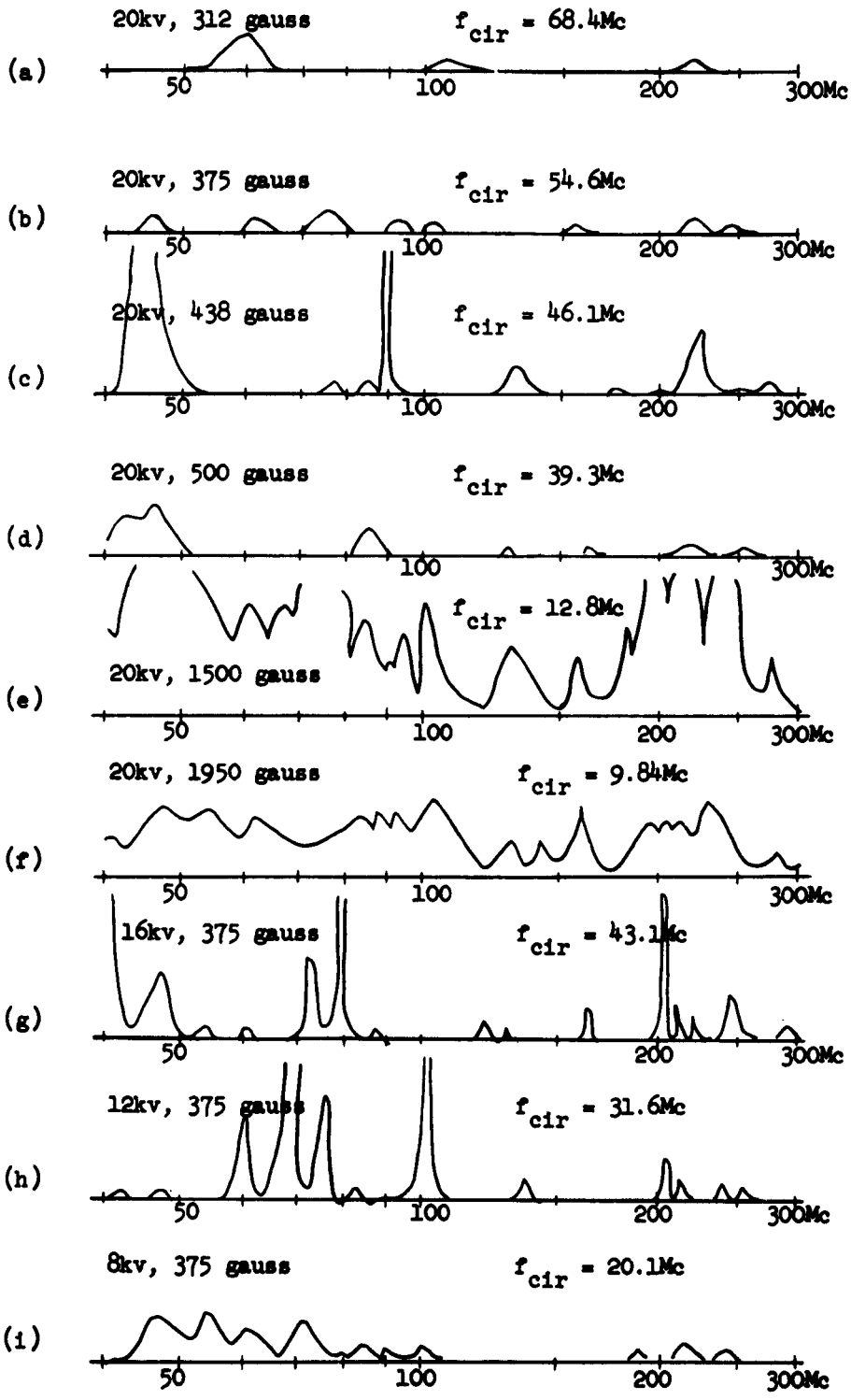

Fig. 13.--Noise spectra for tungsten filament at 5.1×10^{-5} mm of Hg (H_2 gas, SS-2.4).

formation of strong bunches. According to Fig. 13, a strong bunch may be formed at 20 kv, 440 gauss and at 14 kv, 375 gauss. These combinations exactly correspond to the second noise peaks of the noise curves in Fig. 7 in spite of the difference in the gas pressures in the two cases. Since there is a noise peak in the high-field region (see Fig. 13-3), we might expect that bunching action also takes place there. A possible plasma formation, which changes the effective cathode position, may be responsible for the broad-peak characteristic in the higher magnetic-field region.

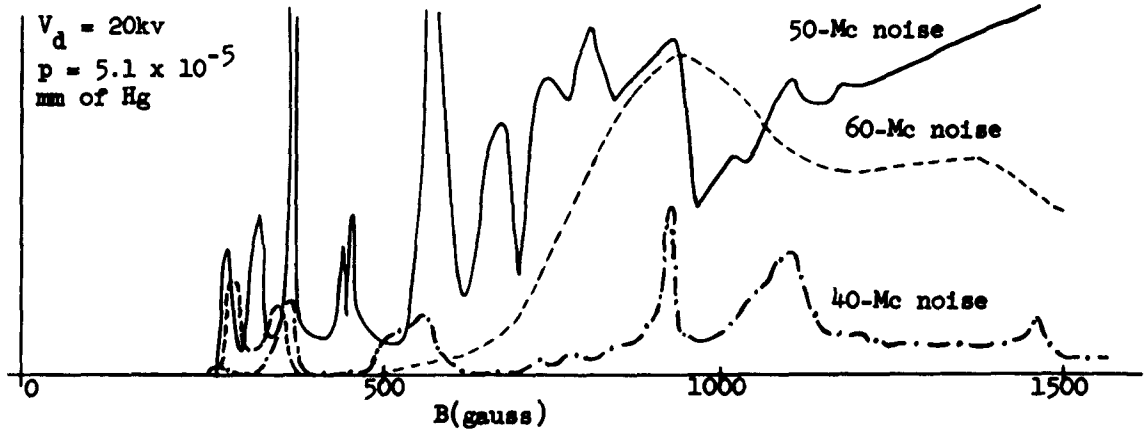

Fig. 14.--Noise at tungsten filament for particular frequencies (5.1×10^{-5} mm of Hg, SS-2.4).

Figure 14 depicts the presence of particular mode frequencies. One resonance frequency is very close to 50 Mc. The number of bunches was explored from the frequency spectra in the higher frequency range. The higher harmonics usually made it difficult to determine the exact frequency. In the cases depicted in Fig. 13 (a) and (e), the conspicuous noise peaks were found in the higher-frequency region: around 1250 Mc for (a) and around 220 Mc for (e). If the circulating frequencies are taken from the calculated values, the ratios of noise-peak to rotation frequency are about 18 and 17, respectively, for the number of bunches. Since the value of $2\pi R_m/d$ is about 17 (where R_m is the mean radius of the interaction

space), the above observations check well with a previous report concerning a similar configuration.[4]

VI. DIAGNOSIS OF PIG DISCHARGE PARTICLES WITH CAGES

Suppose that the secondary-emission yield of the cathode-material shown in Fig. 15 is relatively small and many electrons

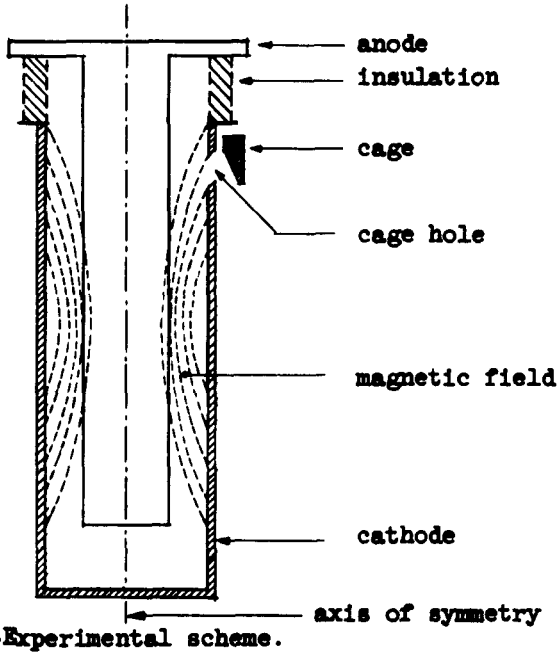

Fig. 15.--Experimental scheme.

are supplied through ionization. Electrons must travel back and forth many times along the lines of magnetic field before their energy allows them to leave the interaction space between cathode and anode.

As the first approximation, the electrons within a volume element bounded by two surfaces of revolution defined by two adjacent curved field-lines, which penetrate the cage-hole and are rotated about the axis of symmetry, may be assumed to be in an equilibrium state. Their density distribution along field lines may be expressed as

$$n = n_0 \exp \left[- e \phi (l)/kT \right] , \qquad (3)$$

where n_0 is the density at the center of the above volume element and $\phi(\ell)$ is the potential for electron (positive) in reference to the center of the same element at the distance ℓ from the reference point. If the velocity distribution is Maxwellian, n_0 should be expressed by the following relation, as far as the dependence on the kinetic-energy component parallel to field lines is concerned:

$$n_0 = \int_0^\infty N(T) \exp\left(-W_{//}/kT\right) dW_{//} \qquad (4)$$

where $W_{//}$ means the component of the energy parallel to the field and $N(T)$ is a function of temperature.

When the cage is biased by $-V_b$ in reference to the cathode potential and the cathode is at a potential $-\phi(\ell_0)$ relative to the center of the volume element, the contribution to the cage current from the same element is proportional to the following integral, which is easily derived from consideration of Eqs. (3) and (4):

$$I_{cage} \propto N(T) \exp\left[-e\phi(\ell_0)/kT\right] \int_{eV_b}^\infty \exp\left(-W_{//}/kT\right) d W_{//}$$

$$\propto \left[N(T)/T\right] \exp\left[-e\phi(\ell_0)/kT\right] \exp\left[-eV_b/kT\right] \qquad (5)$$

The above expression permits the usual method for the measurement of the electron temperature. The only requirement is to get the I_{cage}-V_b characteristics.

It has been implicitly assumed that the impressed voltage between anode and cathode is constant with time. Even if the instantaneous anode voltage changes with time slowly, compared to the period of the electron motion along the magnetic field (so that the distribution of electrons changes with time), the proportionality between I_{cage} and $\exp\left[-eV_b/kT\right]$ never changes; but the proportionality coefficient of Eq. (3) must be replaced by an appropriate integral value averaged with time.

If the secondary-emission yield of the cathode material is quite high and a high vacuum is used, secondary electrons comprise

two groups. One is the true secondary group and the other is the rediffused electron group.[10] True secondary electrons usually have low energy below a few tens of electron volts and their energy distribution is nearly independent of the energy of the primary electrons. Thus these electrons would be expected to constitute a low-temperature group of electrons. The others, rediffused electrons, have usually energies of the same order as the primaries and the directions of their velocities are strongly scattered; these electrons tend to constitute a high kinetic-temperature group. Strong bunching action may promote temperature equalization between the two groups.

Some consideration should be given to the relaxation time in which the particles interact with each other through two-particle interactions. The result of a calculation using the relations given by Spitzer[11] indicates that the relaxation time is much too long to be of any use for plasma heating by means of a P.I.G.-discharge. Thus if we are to achieve plasma heating in a P.I.G. discharge it must be done through a collective interaction similar to that described above.

VII. CAGE-CURRENT CHARACTERISTICS

For investigating the effect of a bias voltage on the current to a probe, a cage is to be preferred to a filament, because secondaries are eliminated, and because the effective surface area does not change appreciably. The wave patterns on the oscilloscope for the cage potential are similar to those for the anode noise in Fig. 10 (a) to (e), and they do not change appreciably according to whether the anode condenser is inserted or not.

Typical examples for the no-bias cage-current characteristics are shown in Fig. 16. If the anode voltage is increased from zero for a fixed magnetic field (the current of the coil is fixed), the current at Cage 2, which is farther from the center, builds up at first and then decreases. The higher voltage is required for the building-up of the Cage 1 current as well as for that of the Cage 2 current, corresponding to the higher magnetic field. This tendency

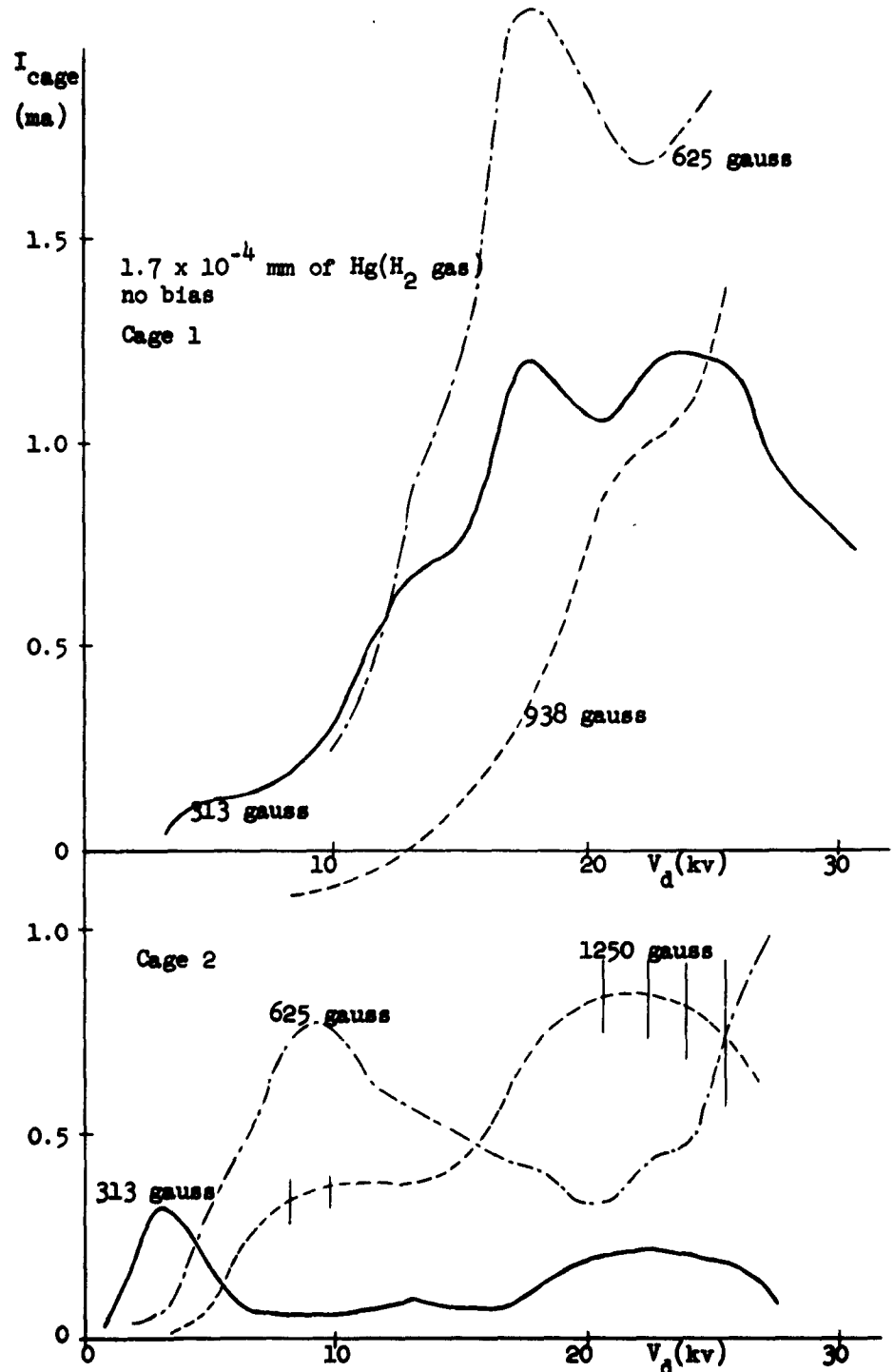

Fig. 16.--Cage current vs voltage for (88-2.4).

suggests that the path of the P.I.G.-discharge current along the magnetic-field lines may be modified a little by the circulating electron-beam current. A simple calculation shows that the absolute value of the field caused by the circulating current amounts to only a fraction of 1 per cent of the externally applied field. However, the percentage may increase appreciably if only the radial component of the field is considered, which is mainly responsible for the curvature modification. This phenomenon makes the measurement of the electron temperature difficult.

Figure 17 plots the cage-current characteristics versus magnetic field, and also illustrates the effect of the cage bias voltage. It can be easily seen that a high electron kinetic

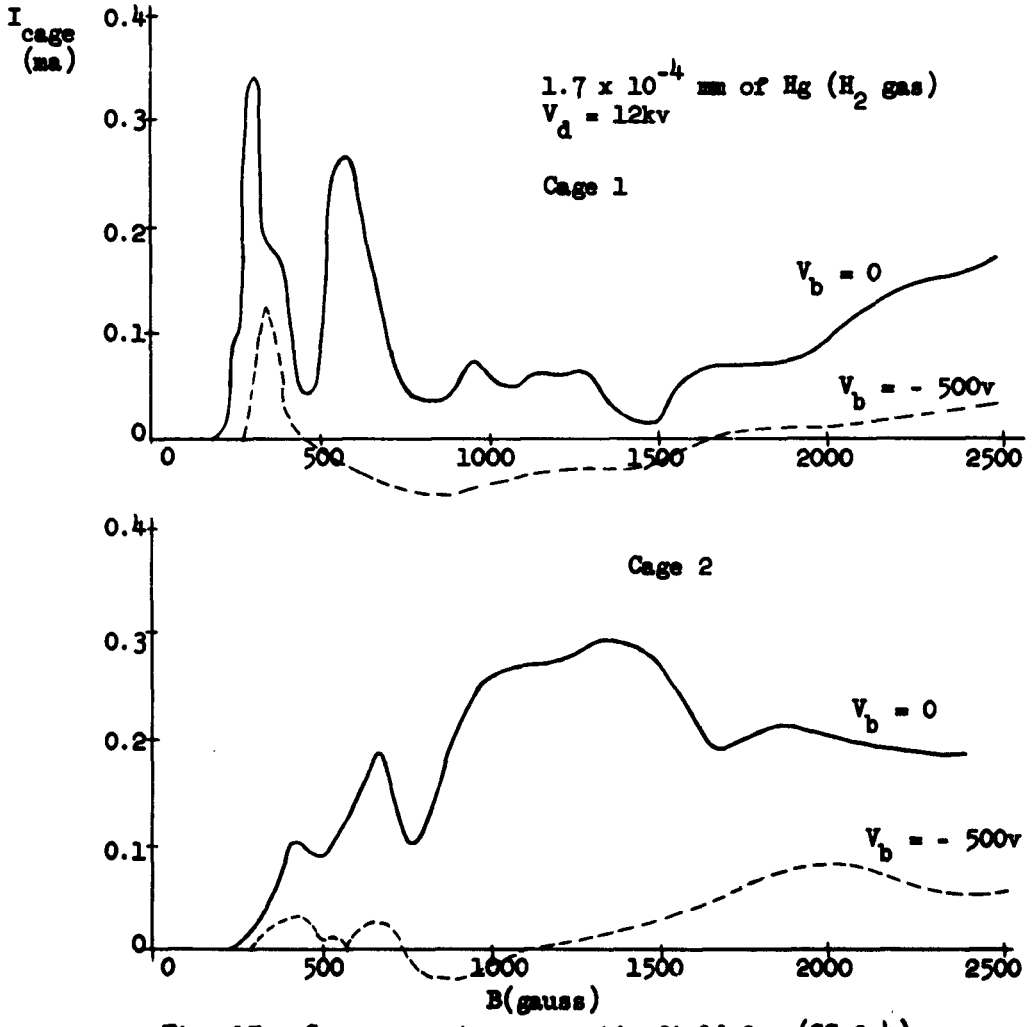

Fig. 17.--Cage current vs magnetic field for (88-2.4).

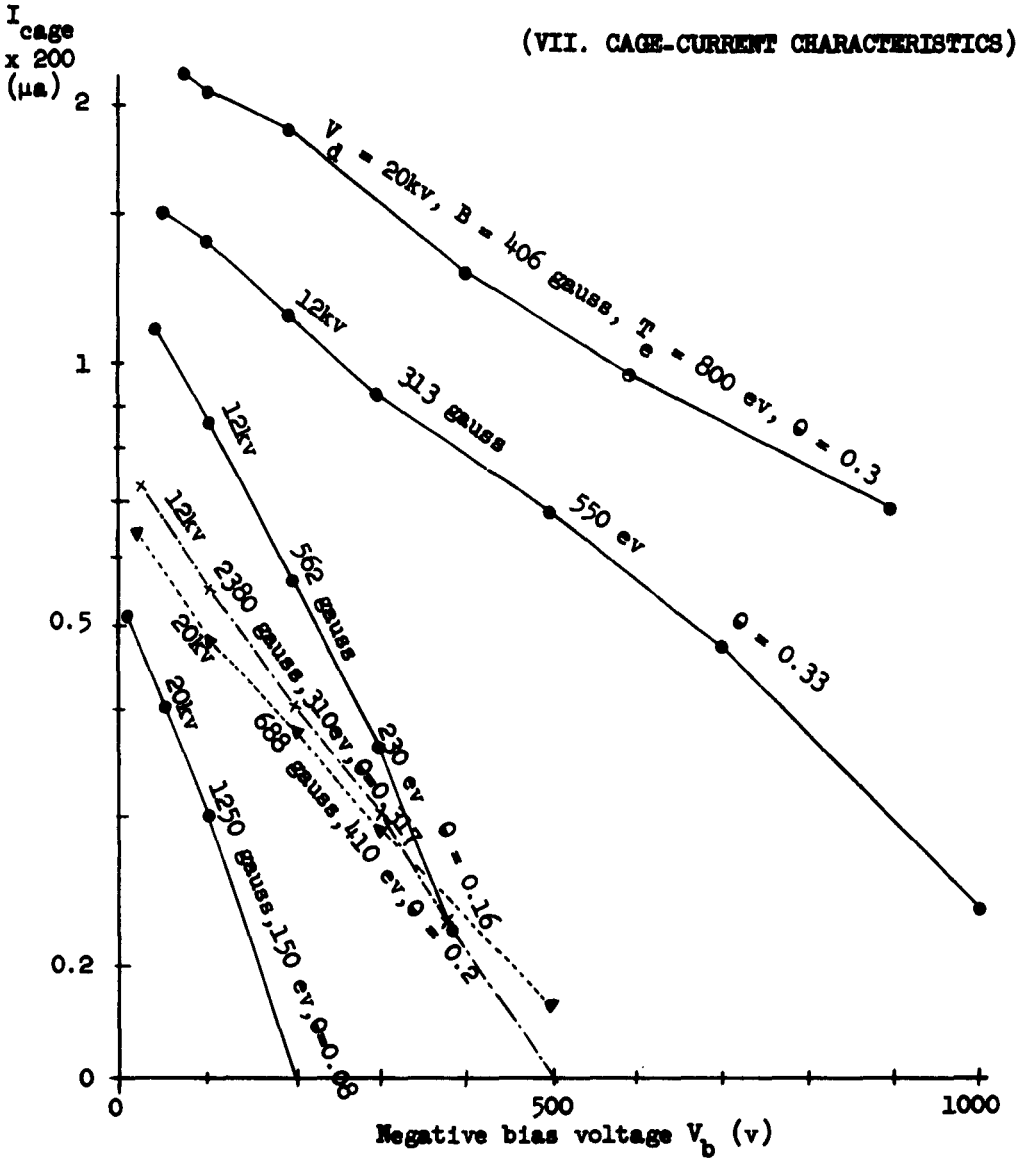

Fig. 18.--Examples of cage-current bias-voltage characteristics.

temperature is produced at specific values of both low and high magnetic field.

Some examples of the bias-voltage dependence of the cage current are shown in Fig. 18, where the electron kinetic temperatures are calculated from the curve slopes and recorded. The values of the electron temperature and the cage current at zero bias voltage allow the approximate estimate of the position where the interaction between electrodes takes place, if the electron

density at the place is assumed to be around the same as that for a laminar-flow state (for example, see Ref. 3). The results are also recorded in Fig. 18 in terms of θ, which expresses the ratio of the potential at the interaction place (where the cage current originates) to the anode potential, with the cathode potential taken as zero. A higher temperature for a given anode voltage corresponds to a larger value of θ. However, the position is still always in the vicinity of the cathode for the (SS-2.4) device. Similar values of θ are obtained from the data for the (SS-1.1) device, for which the cage current was observed only in the higher magnetic-field region. As for the (Al-2.45) device, the values of θ are found to be less than about 0.16. This result indicates that the turbulence occurs near the cathode. These results are consistent with a slipping-stream hypothesis.

VIII. ELECTRON KINETIC TEMPERATURE

The electron kinetic temperature measured with the cage current is particularly interesting if attention is directed to the possibility of plasma heating. An electron may, for example, get a sufficiently high kinetic energy for fusion purposes when it moves along the curved field lines of a PIG discharge. Some fundamental information related to this possibility will be given below.

A typical example of the magnetic-field dependence of the temperature under fixed anode voltage is illustrated in Fig. 19, where two conspicuous peaks are found. One of the peaks is found in a low-magnetic-field region and the other is in a region of high field. This tendency is the same as the I-V and noise characteristics described previously. (For example, Fig. 9 was obtained under very similar conditions.)

The peak in the lower field region is usually observed at a point close to the peak-noise condition, which is found if the anode condenser is not inserted. The high-temperature and noise peaks never coincide, however, which can be explained by the fact that the high-voltage anode noise causes the electrons to be drained

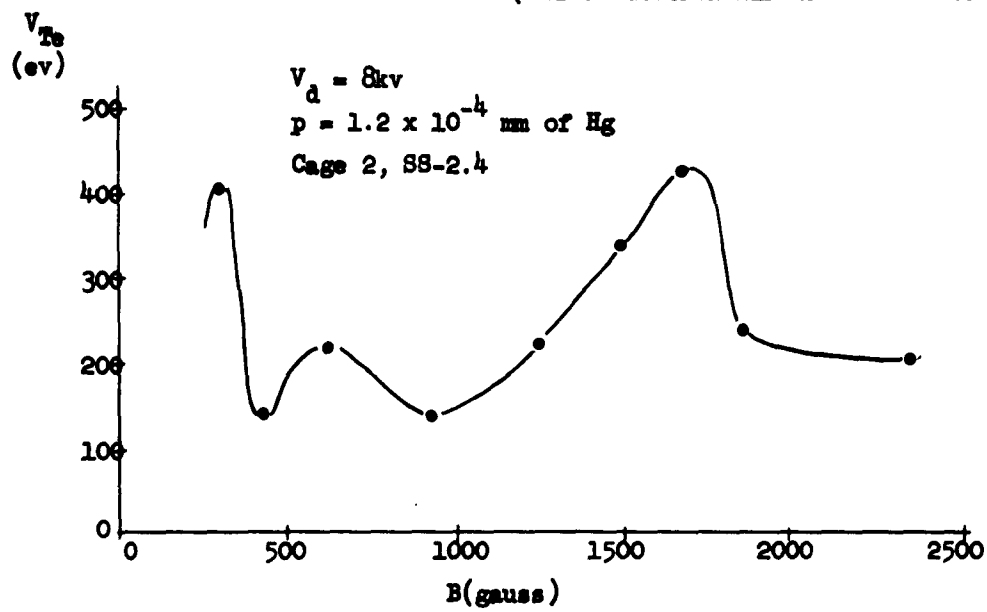

Fig. 19.--Magnetic-field dependence of electron temperature under a fixed anode voltage.

out, so that the time required for an electron to get to a high temperature through mutual interaction is reduced. Several comparisons between the temperatures measured with and without the anode condenser were made and the result shows that no appreciable difference is found between them. A little difference is found, however, between the temperatures measured with different cages.

The peak temperature found in the lower magnetic-field region is plotted in Fig. 20, which also shows the corresponding B-V_d characteristics. The data include those taken with and without the anode condenser. The B-V_d characteristic corresponds approximately to B^2/V_d = constant, as pointed out in the previous section concerning the anode noise. The peak value of V_T increases approximately linearly with anode voltage. A sharp temperature peak is one of the features for the temperature characteristic in the lower field region.

A broad peak is observed in the higher field region. This broad peak characteristic, as previously discussed, may be caused by a variable plasma layer which changes the effective separation

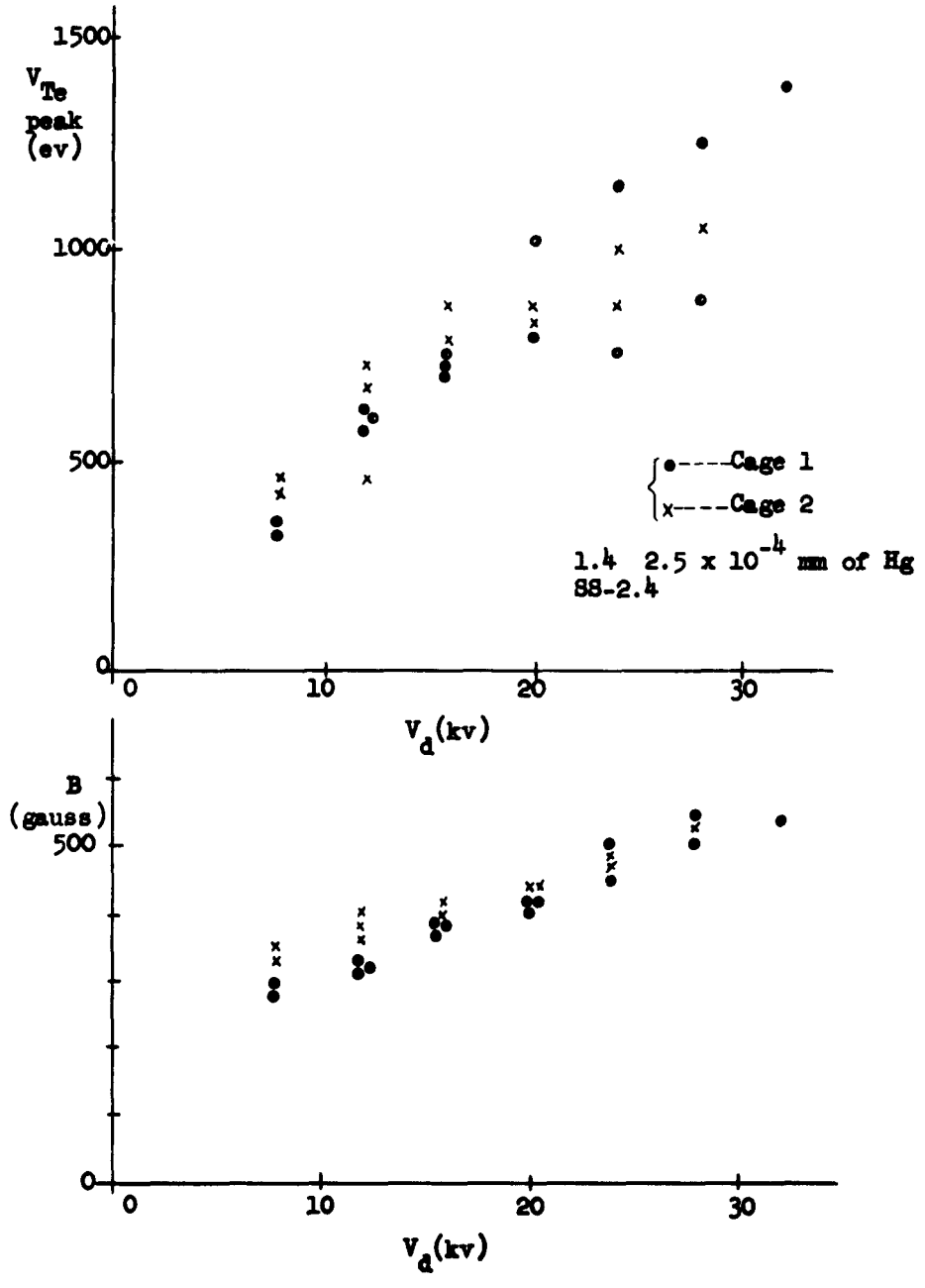

Fig. 20.--Characteristics for the peak electron temperature in the lower magnetic-field region (88-2.4).

distance between anode and cathode.

Some of the data of the aluminum cathode are illustrated in Figs. 21 and 22. They are examples of the characteristics with a

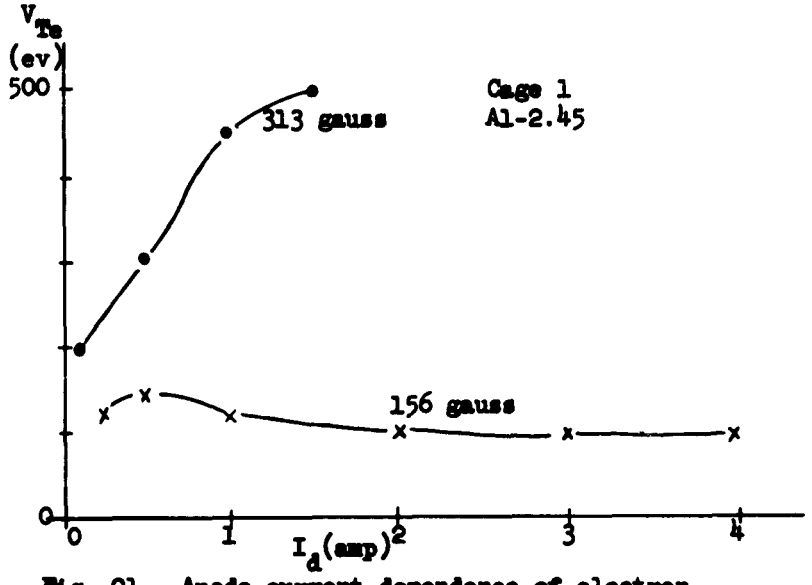

Fig. 21.--Anode-current dependence of electron temperature for Al-cathode.

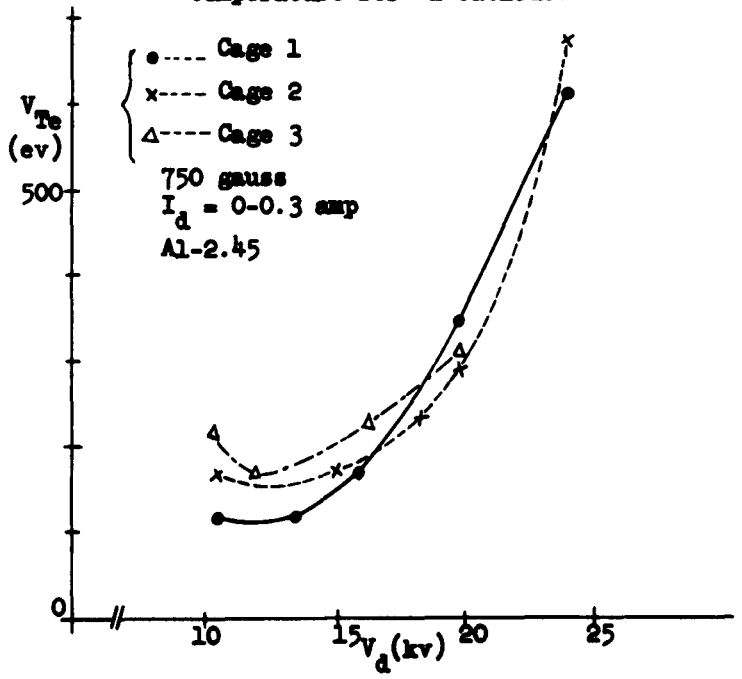

Fig. 22.--Anode-voltage dependence of electron temperature for Al-cathode.

fixed magnetic field. The curve for 156 gauss shows that the peak temperature appears at the threshold of a strong magnetron-action (that is, the current increases owing to strong ordered motion), but the temperature does not increase, probably because the high-temperature electrons are removed before their temperature can increase any further. The difference between the temperatures observed with different cages is not significant.

The correlations among anode noise, frequency spectra for tungsten-filament noise, no-bias cage-current characteristics, and electron-kinetic temperature show that a single phenomenon is probably responsible for all effects, and that this phenomenon can be interpreted in terms of bunching action.

Additional evidence for the coincidence between a high kinetic temperature and a strong bunching action is provided from the data of a device with rf anode structure and Al-cathode. It was easier to obtain a high kinetic temperature for the device with an rf structure than for the one with a smooth-bore anode, which can be correlated with the fact that bunches are more easily formed when an rf structure is present.

IX. CATHODE DISSIPATION

The power dissipated at the cathode and the anode were measured by observing the increase in temperature of the cooling water. Because of the variability of the water flow and the comparatively small amount of energy loss, reliable data are scarce for the (SS-2.4) device. They are tabulated in Table 2. The rate of the cathode dissipation is usually of the order of 40 per cent and is clearly higher for the peak electron-temperature condition described in Fig. 20.

As for the (SS-1.1) device, the results are shown in Figs. 23 and 24. If the observation is made under a fixed anode current, the different states of operation, corresponding to the different humps of Figs. 5 and 6 (V_d-I_d curves), have different rates of the cathode dissipation. Along the curve corresponding to one particular

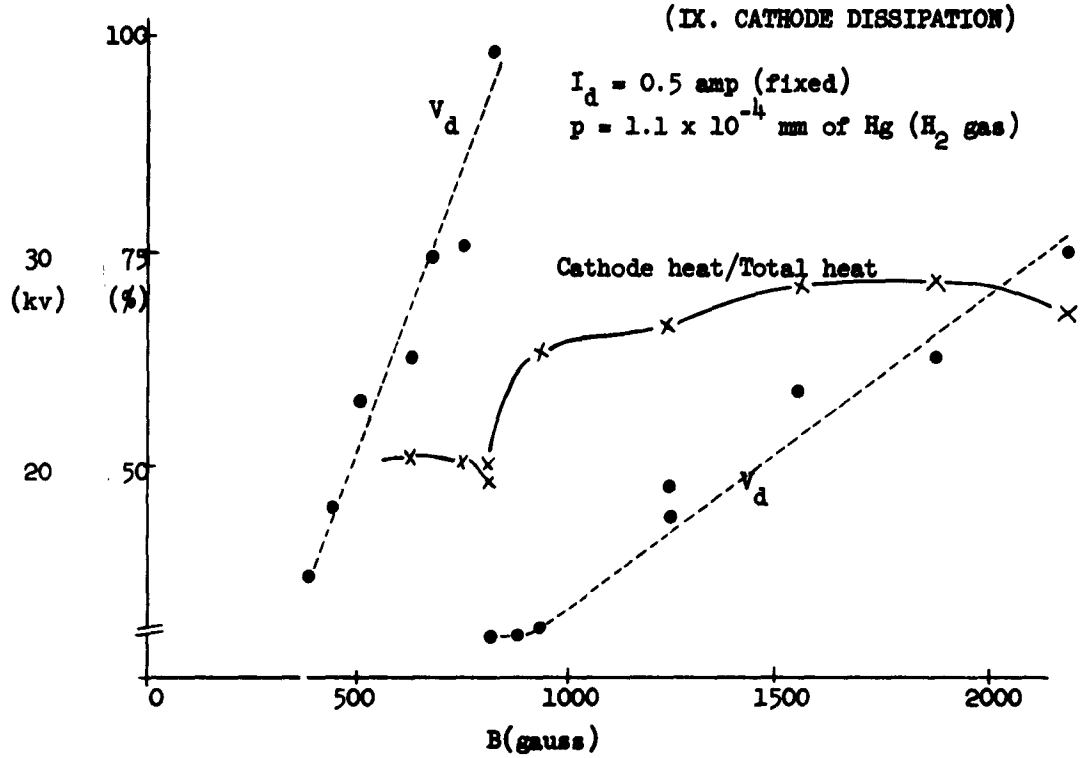

Fig. 23.--Cathode dissipation vs magnetic field for (SS-1.1)

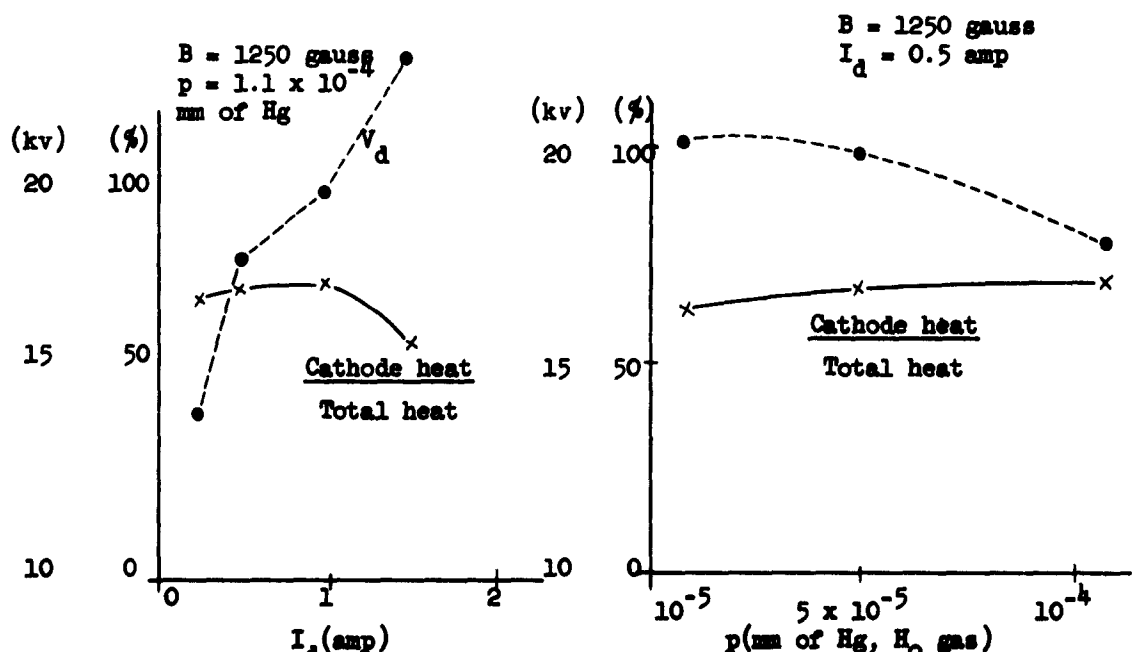

Fig. 24.--Cathode dissipation vs current and pressure for (SS-1.1).

TABLE 2.--Cathode dissipation for (88-2.4).

V_d (kv)	B (gauss)	Cathode heat / Total heat (%)	P (mm of Hg)
24	438	47.4	2.2×10^{-4}
24	488	42.4	2.2×10^{-4}
28	500	47.2	2.2×10^{-4}
28	519	41.2	2.2×10^{-4}
24	475	44.3	2.4×10^{-4}
24	313	37.6	4.8×10^{-4}

mode, the rate of the cathode dissipation amounts to 70 per cent.

The regions of high cathode dissipation (Fig. 25) are correlated to the regions of high temperature (Fig. 21). For the aluminum cathode, the rate of cathode dissipation is quite low, of the order of a few tens of 1 per cent. In other words, a higher yield of secondary emission from the cathode corresponds to a lower voltage and therefore correspondingly lower turbulent velocities.

Figures 23 and 25 both indicate that the magnetron operation may take place in quite different space-charge configurations at the different regions of the magnetic field. The critical values of the field may depend on the device itself.

X. OPTIMIZATION OF THE SELF-INTERACTION OF THE ELECTRONS

A. SIMPLE THEORY FOR OPTIMUM ANODE VOLTAGE AND MAGNETIC FIELD FOR THE SELF-INTERACTION OF ELECTRON BEAM

The guiding center of an electron obeys two kinds of motion: a drift perpendicular to the crossed field (with a velocity proportional to V_d/B) and a P.I.G.-discharge motion along the field lines (for which the oscillation period is inversely proportional to $\sqrt{V_d}$). Since charge accumulation is necessary for a strong

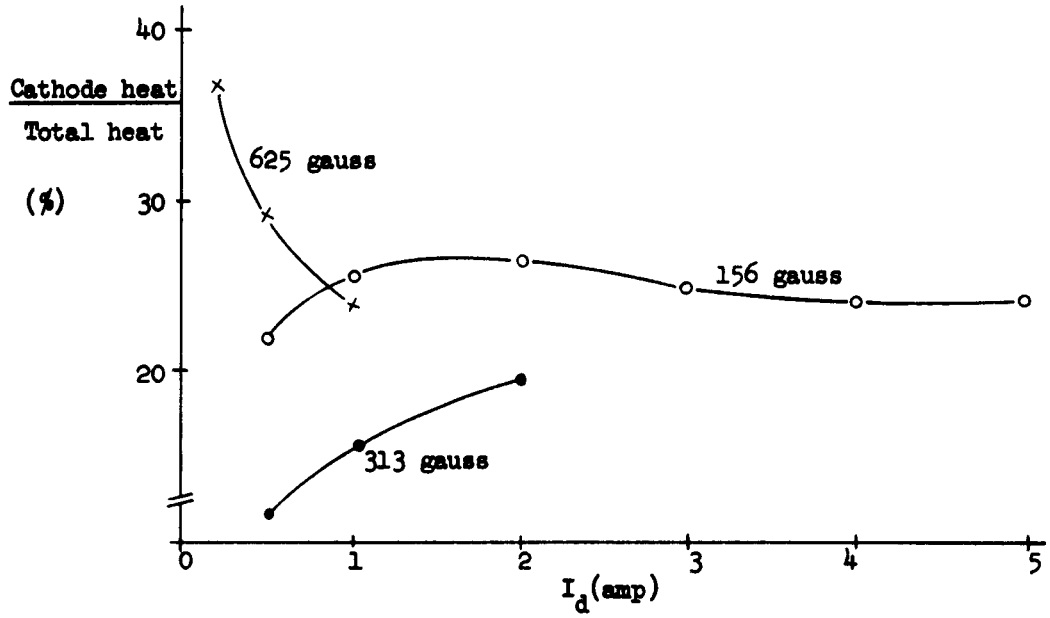

Fig. 25.--Cathode dissipation vs current for (A1-2.45).

interaction of the electrons, it may be required for an electron to travel as long a distance as possible while it stays at the active interaction space. In other words, the product of V_d/B and $V_d^{-1/2}$ should be as large as possible, unless otherwise limited. The resulting factor, $\sqrt{V_d/B}$, is easily found to be proportional to $\sqrt{r_c}$, where r_c is the cyclotron radius for electrons in the interaction space with no space charge.

A second requirement is that the total volume occupied by electrons should be made as large as possible. Clearly the volume occupied by guiding centers is proportional to $(d - 2r_c)$, where d is the separation distance of the electrodes.

We therefore expect the maximum interaction when the product $\sqrt{r_c}(d - 2r_c)$ is maximized. Thus the following relation is introduced for the optimum interaction:

$$r_c = d/6 \qquad (6)$$

which reduces to

$$B_f = \sqrt{\frac{6\,V_f}{\eta d^2}} \qquad (7)$$

where $\eta = e/m$. The voltage given by Eq. (7) corresponds to one third of the cutoff voltage of a planar magnetron. Equation (6) can also be written

$$d = 6\,r_c \simeq 2\pi\,r_c$$

As has been described in Sec. V, the distance between bunches may be of the same order as the separation distance between electrodes. Equation (6) gives the condition that the bunch distance is approximately equal to the length of the cyclotron circumference of an electron.

A comparison of the theory with the experimental results is shown in Fig. 26. The peak electron temperature (from Fig. 20) is assumed to be a measure of the peak interaction.

B. RELEVANCE OF THE THEORY OF CROSSED-FIELD TUBES WITH THICK BEAMS

According to the theory of the diocotron effect for a slipping beam[12] the rate of growth of a disturbance with distance is a maximum for the approximate condition

$$\frac{2\pi}{\lambda_b}\,\alpha \simeq 0.8 \qquad (8)$$

where α is the beam thickness and λ_b is the wavelength of the growing space-charge wave.

For an estimate of α, the space-charge picture in a laminar-flow state may be considered. As has been described in Sec. X-A, the optimum anode voltage is about 1/3 of the cutoff voltage. Under this condition, α is roughly equal to r_c, the cyclotron radius in the interaction space without space charge;[3] λ_b may be assumed to be approximately equal to d. With the above considerations we derive from Eq. (8) the relation between the anode voltage and magnetic field for maximum growth:

$$B_f = \sqrt{\frac{2\pi V_f}{0.8\,\eta d^2}} \qquad (9)$$

The results calculated from Eq. (9) are also shown in Fig. 26. Good agreement with the experimental data is found, despite the fact that the assumptions were based on a planar magnetron model.

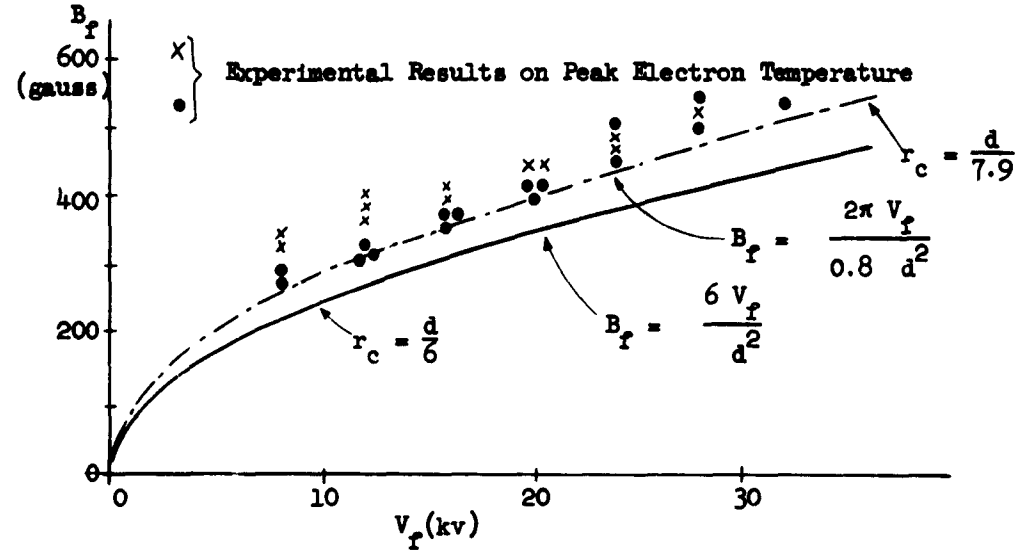

Fig. 26.--Optimum relation between V_f and B_f for magnetron action.

C. AN APPLICATION

The preceding results give a method for the determination of the operating voltage and magnetic field in the lower magnetic-field region. Suppose the rf structure has a resonant frequency of f_a and a space-charge wavelength λ_s, which is determined by the periodicity of the rf structure. The synchronism condition for the electron drift velocity gives approximately

$$\lambda_s f_a = V_d/B_d$$

and in accordance with Eq. (9)

$$V_d = (0.8/2\pi)\ \eta d^2 B^2$$

The above expressions determine the optimum V_d and B for a given structure. (Though best operation is expected for the structure with $\lambda_s = d$, where d is the anode-cathode spacing, the voltage and magnetic field can be optimized even when this condition is not satisfied.) A relatively successful anode structure has been designed at this Laboratory for which $f_a = 145$ Mc, $\lambda_s = 5.8$ cm, and d = 1 cm. The formulas give B = 380 gauss and $V_d = 3.2$ kv as the result from the above relations. These values coincide well with the optimum operating condition obtained experimentally.[2]

XI. CONCLUSION

The use of a stainless-steel cathode has provided a better understanding of cold-cathode magnetrons.

The kinetic temperature of the electrons in the space-charge sheath of a plasma magnetron appears to be produced mainly by the turbulence due to the diocotron effect, which leads to the formation of bunches. Calculations indicate that scattering owing to collisions is not sufficient to randomize the ordered motion of the P.I.G. discharge.

There are at least two kinds of modes with which the electrons can achieve a peak kinetic temperature. One mode is related to a relatively low magnetic field. Equation (7) or (9) gives the optimum relations among the anode voltage, the magnetic field, and the electrode separation. The other mode is concerned with a relatively higher magnetic field, where the cyclotron radius of an ion decreases appreciably, so that a plasma may be formed above the surface of the cathode, and the optimum voltage is approximately proportional to the magnetic field.

The conditions for peak temperature are intimately related to bunch formation and maximum magnetron-type amplification. The wavelength of the space-charge wave in the interaction space is found to be the same as the separation distance between electrodes.

It has been proved experimentally that the previous theory for the growth of a space-charge wave owing to the diocotron

effect for a thick slipping-stream beam gives accurate results.[12]

Sufficient secondary emission can lower the operating anode voltage for a given current. If the rf structure of the anode does not coincide with the mode of the smooth cylindrical structure, it may be expected that some jump phenomena between modes occur, which correspond to bumps in Figs. 5 and 6.

There are still some important problems to be considered before either of the electrodes can be replaced with a plasma for the purpose of studying an ion-sheath that might exist. The mode in the higher magnetic-field region has not been explored sufficiently because of the limitation of the voltage or the magnetic field available. The higher magnetic-field region is probably the more interesting one with respect to plasma confinement problems.

DISTRIBUTION LIST
Contract No. AF 19(628)-334

ORGANIZATION	NO. COPIES
AFMTC (AFMTC Technical Library-MU-135) Patrick AFB, Florida	1
AUL Maxwell AFB, Alabama	1
OAR (RROS, Col. John R. Fowler) Tempo D 4th and Independence Avenue Washington 25, D. C.	1
AFOSR, OAR (SRYP) Tempo D 4th and Independence Avenue Washington 25, D. C.	1
ASD (ASAPRD-Dist) Wright-Patterson AFB, Ohio	1
RADC (RAALD) Griffiss AFB, New York ATTN: Documents Library	1
AF Missile Development Center (MDGRT) Holloman AFB, New Mexico	1
Hq, OAR (RROSP, Maj. Richard W. Nelson) Washington 25, D. C.	1
ARL (ARA 2) Library, ARL 2292, Building 450 Wright-Patterson AFB, Ohio	1
Commanding General USASRDL Ft. Monmouth, New Jersey ATTN: Tech Doc. Ctr SIGRA/SL-ADT	1
Department of the Army Office of the Chief Signal Officer Washington 25, D.C. ATTN: SIGRD 4a-2	1
Commanding Officer Diamond Ordnance Fuse Laboratories Washington 25, D.C. ATTN: ORDTL 012	1
Redstone Scientific Information Center U. S. Army Missile Command Redstone Arsenal, Alabama	1
Office of Scientific Intelligence Central Intelligence Agency 2430 E Street, N.W. Washington 25, D.C.	1
ASTIA (TIPAA) Arlington Hall Station Arlington 12, Virginia	10
Scientific and Technical Information Facility P. O. Box 5700 Bethesda, Maryland ATTN: NASA Representative (S-AK/DL)	1
Director Langley Research Center National Aeronautics and Space Administration Langley Field, Virginia	1
Chief, Bureau of Naval Weapons Department of the Navy Washington 25, D.C. ATTN: DLI-31	2
Director (Code 2027) U.S. Naval Research Laboratory Washington 25, D.C.	2
Director, USAF Project RAND The Rand Corporation 1700 Main Street Santa Monica, California THRU: AF Liaison Office	1
AFCRL, OAR (CRERA - Stop 39) L. G. Hanscom Field Bedford, Massachusetts	10
U.S. Army Aviation Human Research Unit U.S. Continental Army Command P.O. Box 428 Fort Rucker, Alabama ATTN: Major Arno H. Eliasson	1
Library Boulder Laboratories National Bureau of Standards Boulder, Colorado	2
Institute of the Aerospace Sciences, Inc. 2 East 64th Street New York 21, New York ATTN: Librarian	1
Massachusetts Institute of Technology Research Laboratory Building 26, Room 327 Cambridge 39, Massachusetts ATTN: John M. Hewitt	1
Aldermen Library University of Virginia Charlottesville, Virginia	1
Defence Research Member Canadian Joint Staff 2450 Massachusetts Avenue, N.W. Washington 8, D.C.	1
Directorate of Development Planning DCS Research & Technology Hq USAF (AFRDP-2, Michael Lerouge) Washington 25, D.C.	1
RADC (RALTP, A. Wojcik) Griffiss AFB, New York	1
RADC (RALBR, LeonardStrauss) Griffiss AFB, New York	1
ASD (ASRMPE, Mr. Richard Rivir) Wright-Patterson AFB, Ohio	1
Advisory Group on Electron Devices (AGED) Office of the Director of Defense Rand&E 346 Broadway, 8th Floor New York 13, New York	4
Bell Telephone Laboratories, Inc. Whippany Laboratory Whippany, New Jersey ATTN: Technical Information Library	2
Technical Library G.E. TWTProduct Section 601 California Avenue Palo Alto, California ATTN: Verna Van Velzer, Librarian	1
General Electric Advanced Electronics Center Tompkins County Airport Ithaca, New York ATTN: Mr. F. M. Perry	1
Estel-McCullough, Inc. 301 Industrial Way San Carlos, California ATTN: Stella R. Vetter, Librarian	1
Sylvania Electric Products, Inc. Electronic Defense Laboratory 123 N. Whisman Road Mountain View, California ATTN: Library	1
Division of Sperry Rand Corporation Sperry Gyroscope Company Great Neck, Long Island, New York ATTN: Florence W. Turnbull, Eng. Librarian	1
General Electric Company, Power Tube Department Electronic Components Division Building 269, Room 209 One River Road Schenectady 5, New York	1
General Telephone & Electronics Laboratories, Inc. Bayside Laboratories Bayside 60, New York ATTN: D. Lasare, Mgr., Proj. Adm.	1
Estel-McCullough, Inc. 790 San Mateo Avenue San Bruno, California ATTN: Donald H. Preist	1
Varian Associates 611 Hansen Way Palo Alto, California ATTN: Dr. Richard B. Nelson	2
Varian Associates 611 Hansen Way Palo Alto, California ATTN: E. W. Herold Vice President, Research	1
Lockheed Aircraft Corporation Missiles & Space Division Technical Information Center 3251 Hanover Street Palo Alto, California ATTN: W. A. Kocumpih, Manager	1
AVCO Manufacturing Company 2385 Revere Beach Parkway Everett 49, Massachusetts ATTN: Dr. A. R. Kantrowitz	1
Philips Laboratories Division of North American Philips Co., Inc. Irvington on Hudson, New York ATTN: William F. Arnott, Security Officer	1
Research Technology Associates, Inc. 100 Lodge Drive Electronic Park at Avon Avon, Massachusetts ATTN: J. Bakalian	1
ARO, Inc. AEDC Library Arnold Air Force Station, Tennessee	1
Raytheon Company Norwood Plant 455 Providence Highway Norwood, Massachusetts ATTN: L. C. Edwards	1
Rochedyne 6633 Canoga Avenue Canoga Park, California ATTN: Dr. R. H. Boden, Department 564-370	1
Aero Chem Research Laboratories, Inc. P. O. Box 12 Princeton, New Jersey ATTN: Dr. Caiesto	1
Litton Systems, Inc. 336 N. Foothill Road Beverly Hills, California ATTN: Space Sciences Laboratory	1
Hughes Research Laboratories Malibu, California ATTN: Dr. M. E. Currie	1
Westinghouse Electric Corporation P. O. Box 284 Elmira, New York ATTN: D. C. Buch, Head Microwave Research & Development Section	1
American Systems Incorporated 1625 East 126th Street Hawthorne, California ATTN: M. D. Adcock, Director Electromagnetic Systems Division	1
Lunde Company 1500 Polco Street Speedway 24, Indiana ATTN: Dr. M. Born	1
General Telephone & Electronics Laboratories, Inc. Microwave Physics Laboratory 1015 Corporation Way Palo Alto, California ATTN: Librarian	1
S-F-D Laboratories, Inc. 800 Rahway Avenue Union, New Jersey	1
F. J. Liberatore, Code 7420 U.S. Naval Research Laboratory Washington 25, D.C.	1
New York University Institute of Mathematical Sciences 25 Waverly Place, Room 802 New York 3, New York ATTN: Dr. Morris Kline	1
Stanford University Stanford Electronics Laboratories Stanford, California ATTN: Dr. Dean A. Watkins	1
Stanford University Microwave Laboratory W. W. Hansen Laboratories of Physics Stanford, California ATTN: Dr. Marvin Chodorow	1
California Institute of Technology 1201 E. California Street Pasadena, California ATTN: Dr. S. S. Penner	1
Polytechnic Institute of Brooklyn Microwave Research Institute 55 Johnson Street Brooklyn, New York ATTN: Dr. N. Marcuvitz	1
The Ohio State University Department of Physics 174 W. 18th Avenue Columbus 10, Ohio ATTN: Prof. M. L. Poyl	1
University of Maryland College Park, Maryland ATTN: Dr. J. M. Burgers	1
Cornell University Ithaca, New York ATTN: W. R. Ware	1
Electrical Engineering Research Laboratory University of Illinois Urbana, Illinois ATTN: Dr. A. A. Dougal	1
Stevens Institute of Technology Hoboken, New Jersey ATTN: Dr. Boothe	1
University of Mississippi University, Mississippi ATTN: Mr. Thomas Tullos	1
Hq. AFCRL, OAR (CRRCPS, S. Shevchenko) L. G. Hanscom Field Bedford, Massachusetts	1

Electronics Research Directorate, Air Force Cambridge Research Laboratories, Office of Aerospace Research, U.S. Air Force, Bedford, Mass.
Rpt. No. AFCRL-63-41, BEHAVIOR OF THE SPACE CHARGE IN A PLASMA MAGNETRON
Interim Report, June 62, 38 p., incl. illus., 12 refs.

Unclassified Report

An analytical and experimental investigation of "plasma" magnetrons with smooth-bore anodes is described. Secondary-emission yield of several materials is investigated and the region in which limiting anode currents are obtained is related to the operation of conventional magnetrons. Basic phenomena caused by Philips-ion-gage discharge particles are described, with particular emphasis on the sheath region. The phenomena underlying the build-up of anode current are elucidated.

1. Electron Tubes
2. Plasma Physics
I. AFCRL Project No. 5634
Task No. 563402
II. Contract AF 19(628)-324
III. Univ. of California, Berkeley, Calif.
IV. Ikeda, Y.
V. ERL Series No. 60, Issue No. 433
VI. Aval fr OTS: $1.25
VII. In ASTIA collection

Electronics Research Directorate, Air Force Cambridge Research Laboratories, Office of Aerospace Research, U.S. Air Force, Bedford, Mass.
Rpt. No. AFCRL-63-41, BEHAVIOR OF THE SPACE CHARGE IN A PLASMA MAGNETRON
Interim Report, June 62, 38 p., incl. illus., 12 refs.

Unclassified Report

An analytical and experimental investigation of "plasma" magnetrons with smooth-bore anodes is described. Secondary-emission yield of several materials is investigated and the region in which limiting anode currents are obtained is related to the operation of conventional magnetrons. Basic phenomena caused by Philips-ion-gage discharge particles are described, with particular emphasis on the sheath region. The phenomena underlying the build-up of anode current are elucidated.

1. Electron Tubes
2. Plasma Physics
I. AFCRL Project No. 5634
Task No. 563402
II. Contract AF 19(628)-324
III. Univ. of California, Berkeley, Calif.
IV. Ikeda, Y.
V. ERL Series No. 60, Issue No. 433
VI. Aval fr OTS: $1.25
VII. In ASTIA collection

Electronics Research Directorate, Air Force Cambridge Research Laboratories, Office of Aerospace Research, U.S. Air Force, Bedford, Mass.
Rpt. No. AFCRL-63-41, BEHAVIOR OF THE SPACE CHARGE IN A PLASMA MAGNETRON
Interim Report, June 62, 38 p., incl. illus., 12 refs.

Unclassified Report

An analytical and experimental investigation of "plasma" magnetrons with smooth-bore anodes is described. Secondary-emission yield of several materials is investigated and the region in which limiting anode currents are obtained is related to the operation of conventional magnetrons. Basic phenomena caused by Philips-ion-gage discharge particles are described, with particular emphasis on the sheath region. The phenomena underlying the build-up of anode current are elucidated.

1. Electron Tubes
2. Plasma Physics
I. AFCRL Project No. 5634
Task No. 563402
II. Contract AF 19(628)-324
III. Univ. of California, Berkeley, Calif.
IV. Ikeda, Y.
V. ERL Series No. 60, Issue No. 433
VI. Aval fr OTS: $1.25
VII. In ASTIA collection

Electronics Research Directorate, Air Force Cambridge Research Laboratories, Office of Aerospace Research, U.S. Air Force, Bedford, Mass.
Rpt. No. AFCRL-63-41, BEHAVIOR OF THE SPACE CHARGE IN A PLASMA MAGNETRON
Interim Report, June 62, 38 p., incl. illus., 12 refs.

Unclassified Report

An analytical and experimental investigation of "plasma" magnetrons with smooth-bore anodes is described. Secondary-emission yield of several materials is investigated and the region in which limiting anode currents are obtained is related to the operation of conventional magnetrons. Basic phenomena caused by Philips-ion-gage discharge particles are described, with particular emphasis on the sheath region. The phenomena underlying the build-up of anode current are elucidated.

1. Electron Tubes
2. Plasma Physics
I. AFCRL Project No. 5634
Task No. 563402
II. Contract AF 19(628)-324
III. Univ. of California, Berkeley, Calif.
IV. Ikeda, Y.
V. ERL Series No. 60, Issue No. 433
VI. Aval fr OTS: $1.25
VII. In ASTIA collection